Cell Reports

Article

Metabolic rescue of α-synuclein-induced neurodegeneration through propionate supplementation and intestine-neuron signaling in *C. elegans*

Graphical abstract

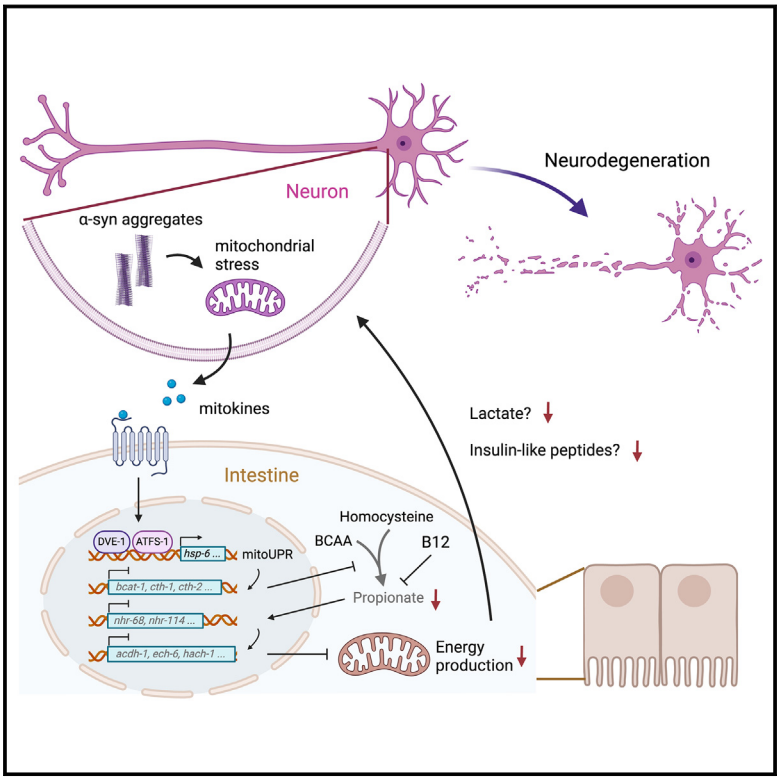

Highlights

- Depleting dietary VB12 or supplementing propionate suppresses neurodegeneration
- Neuronal proteotoxicity triggers mitoUPR and metabolic rewiring in the intestine
- Propionate supplementation reverses PD-associated transcriptomic aberration
- Increased propionate rescues intestinal energy failure and enhances neuronal health

Authors

Chenyin Wang, Meigui Yang, Dongyao Liu, Chaogu Zheng

Correspondence

cgzheng@hku.hk

In brief

Wang et al. find that the short-chain fatty acid propionate suppresses α-synuclein-induced neurodegeneration in a *Caenorhabditis elegans* Parkinson's disease model by regulating interorgan signaling between neuron and intestine. Propionate supplementation reverses intestinal transcriptomic changes triggered by neuronal α-synuclein aggregation and rescues intestinal energy production, which then promotes neuronal health cell-non-autonomously.

Wang et al., 2024, Cell Reports *43*, 113865
March 26, 2024
https://doi.org/10.1016/j.celrep.2024.113865

CellPress

Cell Reports

CellPress
OPEN ACCESS

Article

Metabolic rescue of α-synuclein-induced neurodegeneration through propionate supplementation and intestine-neuron signaling in *C. elegans*

Chenyin Wang,[1] Meigui Yang,[1] Dongyao Liu,[1] and Chaogu Zheng[1,2,*]
[1]School of Biological Sciences, The University of Hong Kong, Hong Kong Special Administrative Region, China
[2]Lead contact
*Correspondence: cgzheng@hku.hk
https://doi.org/10.1016/j.celrep.2024.113865

SUMMARY

Microbial metabolites that can modulate neurodegeneration are promising therapeutic targets. Here, we found that the short-chain fatty acid propionate protects against α-synuclein-induced neuronal death and locomotion defects in a *Caenorhabditis elegans* model of Parkinson's disease (PD) through bidirectional regulation between the intestine and neurons. Both depletion of dietary vitamin B_{12}, which induces propionate breakdown, and propionate supplementation suppress neurodegeneration and reverse PD-associated transcriptomic aberrations. Neuronal α-synuclein aggregation induces intestinal mitochondrial unfolded protein response (mitoUPR), which leads to reduced propionate levels that trigger transcriptional reprogramming in the intestine and cause defects in energy production. Weakened intestinal metabolism exacerbates neurodegeneration through interorgan signaling. Genetically enhancing propionate production or overexpressing metabolic regulators downstream of propionate in the intestine rescues neurodegeneration, which then relieves mitoUPR. Importantly, propionate supplementation suppresses neurodegeneration without reducing α-synuclein aggregation, demonstrating metabolic rescue of neuronal proteotoxicity downstream of protein aggregates. Our study highlights the involvement of small metabolites in the gut-brain interaction in neurodegenerative diseases.

INTRODUCTION

Increasing evidence has highlighted the critical contribution of the gut-brain axis to the development and progression of neurodegenerative diseases.[1] The hundreds of bacterial species in the human gut are essential for food digestion, vitamin synthesis, and the training of the immune system, and changes in the bacterial composition of the gut microbiome have been associated with neurodegenerative diseases. For example, a reduction in the *Prevotellaceae* family of commensal bacteria and an increase in the abundance of *Enterobacteriaceae* correlates with disease severity in Parkinson disease (PD) patients.[2] PD is often characterized by the abnormal accumulation and aggregation of α-synuclein (α-syn) proteins in the dopaminergic (DA) neurons, which leads to mitochondrial dysfunction, oxidative stress, energy failure, and neuronal death.[3] Studies from the mouse PD models with α-syn overexpression confirmed that the gut microbiota were required for the motor deficit and neuroinflammation characteristic of α-syn pathology.[4]

How would the altered microbial composition in the gut contribute to PD pathogenesis? Many studies have focused on the role of short-chain fatty acids (SCFAs), such as acetic acid, propionic acid (PA), and butyric acid, which are produced by the microbiota through the anaerobic fermentation of dietary fibers. Changes in the gut microbiota would lead to the changes in SCFA levels in the enteric metabolome; SCFAs may modulate neuronal health directly by crossing the blood-brain barrier to act on neurons or indirectly by influencing systematic inflammation.[5] However, the effects of SCFAs on neurodegeneration remain controversial.

Germ-free mice overexpressing α-syn had lower levels of SCFA in their fecal samples and reduced motor symptoms than control mice with gut microbiota. Administrating a mixture of SCFAs to germ-free mice led to increased motor impairment and microglial activation,[4] suggesting that SCFAs may be pro-neurodegenerative. However, clinical studies found reduced SCFA levels in the fecal samples of PD patients compared to age-matched healthy individuals.[6] Oral administration of propionate prevented DA neuronal loss and rescued motor deficits in 6-hydroxydopamine-induced PD mice.[7] Propionic acid also protected mesencephalic DA neurons against rotenone-induced toxicity in cellular PD models.[8] Conflicting results were also found for butyrate. Treatment of sodium butyrate in the same 1-methyl-4-phenyl-1,2,3,6-tetrahydropyridine-induced mouse model of PD showed neuroprotective effects in one study[9] but exacerbated neurodegeneration and elevated inflammation in another.[10] Similar inconsistency for the levels and effects of SCFA was also found in Alzheimer disease (AD),[11] and butyrate appeared to ameliorate neurodegeneration in mouse Huntington disease models.[12] The discrepancy among the above studies is

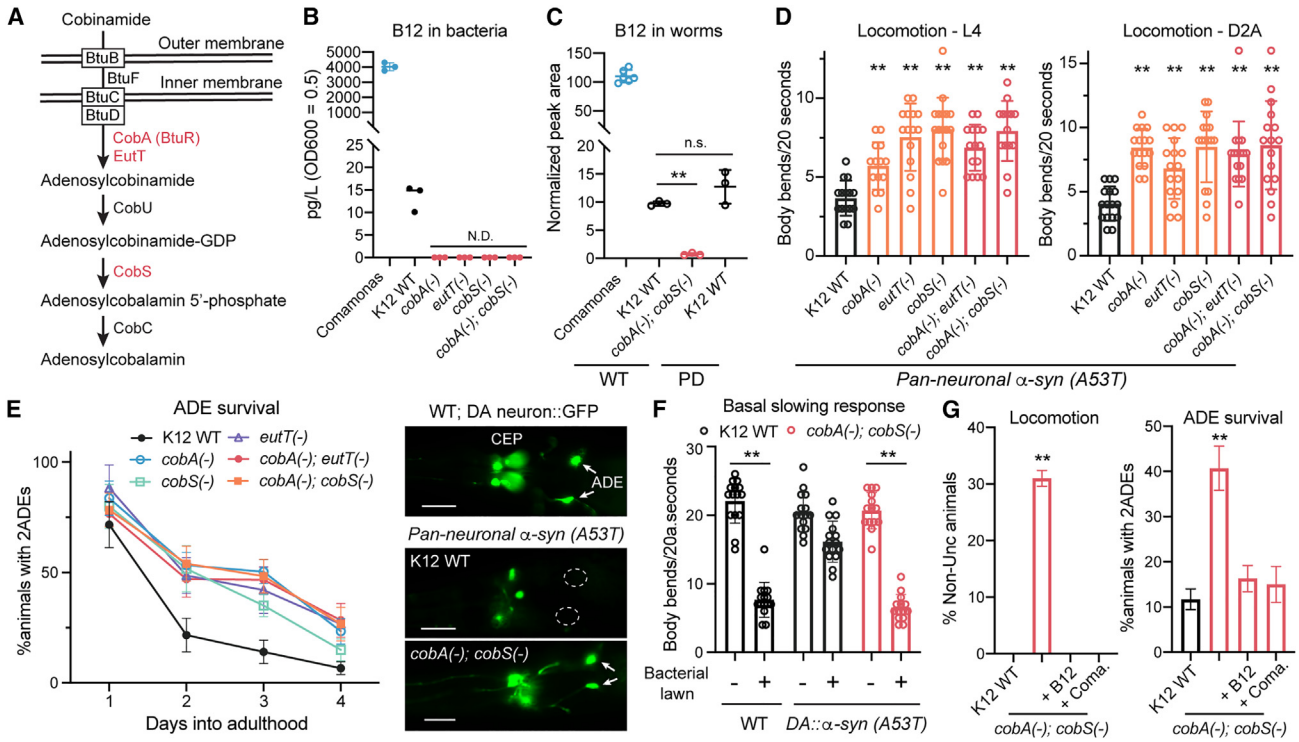

Figure 1. Depletion of dietary B_{12} suppresses α-syn-induced neurodegeneration

(A) Three enzymes (in red) in the salvage-dependent vitamin B_{12} synthesis pathways identified in the screen for proneurodegenerative *E. coli* genes.

(B) The levels of B_{12} determined by LC-MS in the lysate of different bacterial strains. N.D., not detected.

(C) The levels of B_{12} in *C. elegans* WT or PD strains (with pan-neuronal expression of α-syn A53T) fed with different diets.

(D) The number of body bends per 20 s in PD animals fed with different *E. coli* K12 strains at L4 and day 2 adult (D2A) stages.

(E) The number of animals with 2 intact ADE neurons in PD animals fed with different bacteria. The representative images at right showed the presence (arrows) or absence (dashed circles) of ADE neurons. Scale bars, 20 μm.

(F) Movement speed of animals on and off the bacterial lawn in the strain expressing α-syn (A53T) in the DA neurons and fed with various bacterial diets.

(G) Locomotion and ADE survival rate of PD animals with pan-neuronal expression of α-syn (A53T) and fed with *cobA(−); cobS(−) E. coli* supplemented with B_{12} (64 nM) or mixed with Comamonas bacteria (1%).

In (E) and (G), N ≥ 30 for each of at least 3 replicates. Double asterisks indicate $p < 0.01$ in a post-ANOVA Dunnett's or Tukey's test.

often attributed to different types and concentrations of SCFAs used,[13] but the mechanism underlying the effects of SCFAs is not entirely understood.

In this study, using a *Caenorhabditis elegans* model of PD with neuronal expression of human α-syn A53T mutant proteins, we found decreased levels of PA in PD animals compared to the wild type (WT). Increasing the propionate level by removing dietary vitamin B_{12} (which induces propionate breakdown) or through direct supplementation rescued α-syn-induced DA neuron loss and locomotion defects. Surprisingly, the neuroprotective effect of PA is mediated by interorgan signaling between neurons and intestine. α-Syn aggregation in neurons triggered transcriptional changes in the intestine by activating intestinal mitochondrial unfolded protein response (mitoUPR), which resulted in reduced propionate production, and this in turn caused the downregulation of numerous propionate-responsive genes involved in fatty acid and amino acid metabolisms and energy production. Enhancing the production of propionate in the intestine or restoring the intestinal expression of key metabolic regulators downstream of propionate significantly rescued neurodegeneration, suggesting that the metabolic state of the intestine can modulate α-syn-induced neurodegeneration. Therefore, our results support the beneficial effects of SCFAs, such as PA, on preventing neurodegeneration through the gut-brain axis in neurodegenerative diseases.

RESULTS

Depletion of dietary vitamin B_{12} suppresses α-syn-induced neurodegeneration

We previously screened the *Escherichia coli* genome and identified 38 genes that promoted α-syn-induced neurodegeneration in *C. elegans*. Deletion of these bacterial genes suppressed neuronal loss and locomotion defects in PD animals expressing α-syn A53T proteins.[14] Among the 38 *E coli* genes, *cobS*, *cobA* (or *btuR*), and *eutT*, code for key components of the salvage-dependent vitamin B_{12} synthesis pathway. Both *cobA* and *eutT* code for adenosyltransferases that add an adenosyl group to cobinamide, and *cobS* codes for a ribazole transferase that converts adenosylcobinamide-guanosine diphosphate to adenosylcobalamin 5′-phosphate, which is then dephosphorylated to generate adenosylcobalamin (Figure 1A). *E. coli* cannot *de*

novo synthesize cobalamin and only produces vitamin B_{12} through the salvage pathway[15]; thus, the level of B_{12} in *E. coli* is much lower than that in bacterial species (e.g., *Salmonella* and *Comamonas*) that can *de novo* synthesize cobalamin. Using liquid chromatography-mass spectrometry (LC-MS), we confirmed that the *Comamonas* DA1877 strain produced much higher levels of B_{12} than the *E. coli* K12 BW25113 strain (Figure 1B). As expected, B_{12} was not detectable in K12 *cobA(−)*, *eutT(−)*, and *cobS(−)* single mutants or the *cobA(−); cobS(−)* double mutants (Figure 1B). We confirmed that animals fed on *Comamonas* had a much higher level of B_{12} than the ones fed on *E. coli* K12, and no B_{12} was detectable in worms fed with the *cobA(−); cobS(−)* mutants (Figure 1C).

Despite the relatively low level of B_{12} in *E. coli*, depleting B_{12} in the bacterial diet had a strong effect on suppressing the neurodegenerative phenotypes in animals that pan-neuronally expressed α-syn A53T. PD animals fed with K12 *cobS(−)*, *cobA(−)*, and *eutT(−)* single mutants or the *cobA(−); eutT(−)* and *cobA(−); cobS(−)* double mutants had significantly improved motor functions (measured as the number of body bends per 20 s) and increased neuronal survival (measured as the percentage of animals with two intact dopaminergic ADE neurons) (Figures 1D and 1E). Eliminating B_{12} in the diet also largely restored DA neuron functions (measured as food-induced basal slowing response) in another *C. elegans* PD model that expressed α-syn A53T specifically in the DA neurons (Figure 1F).

Moreover, supplementation of vitamin B_{12} to the *E. coli cobA(−); cobS(−)* mutants removed the neuroprotective effects of the diet and led to the same degenerative phenotypes seen in animals fed with WT *E. coli* (Figure 1G). Similarly, mixing the B_{12}-deficient *E. coli* mutants with B_{12}-rich *Comamonas* at a 99:1 ratio restored the strong PD phenotypes (Figure 1G). The above results suggest that B_{12} promotes neurodegeneration in *C. elegans* PD models.

Eliminating vitamin B_{12} does not reduce α-syn aggregation

We next tested whether vitamin B_{12} enhanced neurodegeneration by promoting α-syn aggregation. Through antibody staining, we found that the PD animals fed with WT and *cobA(−); cobS(−)* K12 bacteria showed similar levels and patterns of α-syn staining, and B_{12} supplementation to the *cobA(−); cobS(−) E. coli* diet did not change the α-syn protein signal (Figure S1). α-Syn aggregates were found in both perinuclear clusters and axonal puncta under all treatments. Similar observations were made in animals with pan-neuronal or DA neuron-specific expression of α-syn A53T (Figures S1A and S1B).

We also conducted sequential fractionation of the worm lysate to biochemically analyze α-syn aggregation. The overall protein level of α-syn or its amount in the insoluble fraction did not show significant differences among animals fed with K12 WT or *cobA(−); cobS(−)* mutants (Figures S1C and S1D). B_{12} supplementation did not affect the α-syn levels in different fractions of the lysate either. Thus, the immunofluorescence and the biochemical results both indicate that vitamin B_{12} does not alter neuronal α-syn aggregation. The effects of B_{12} on neurodegeneration are downstream of protein aggregation.

α-Syn aggregation and vitamin B_{12} lead to similar rewiring of metabolic networks

Previous studies found that vitamin B_{12} rewired the metabolic network by repressing the propionate shunt pathway genes and the methionine/S-adenosyl methionine (SAM) cycle genes.[16,17] To our surprise, we found that the same genes were also downregulated in animals with pan-neuronal expression of α-syn A53T, compared to the WT animals (Figures 2A–2C). In fact, more than half of the previously known B_{12}-repressed genes were downregulated in the PD animals, suggesting a significant ($p = 2 \times 10^{-16}$ in a hypergeometric test) overlap between B_{12} and α-syn-induced transcriptomic changes.

Dietary vitamin B_{12} activates the B_{12}-dependent canonical pathway that breaks down propionyl-coenzyme A (CoA), and decreased levels of propionate lead to the silencing of propionate shunt pathway genes.[17] The PD animals showed significant downregulation of *acdh-1*, *ech-6*, *hach-1*, and *hphd-1* (four of the five components in the shunt pathway), which could be caused by the reduction in propionate (Figure 2D). Using gas chromatography-mass spectrometry (GC-MS), we found that the PA level was much lower in PD animals compared to the WT animals (Figure 2E). Importantly, LC-MS results showed that the B_{12} level is similar between PD and WT animals when both are fed with the K12 WT bacteria, suggesting that the low level of propionate in PD animals was not due to abnormal accumulation of B_{12} (Figure 1C). As expected, removing B_{12} from the bacterial diet led to the increase in PA in PD animals (Figure 2E), as previously reported in the WT animals.[18]

What caused the reduction in the abundance of propionate in PD animals? From the transcriptomic analysis, we found that the PD animals showed a 4-fold downregulation of *bcat-1*, which codes for a branched chain amino acid (BCAA) transaminase (BCAT) (Figure 2D). BCAT-1 catalyzes the first step of BCAA breakdown, which leads to the generation of propionyl-CoA.[19] We also observed the reduction in BCAA levels in PD animals compared to the WT animals (Figures S2A–S2C). Thus, the decreased availability of BCAA and the downregulation of *bcat-1* both contributed to the scarcity of propionyl-CoA and propionate in PD animals. Interestingly, BCAT-1 expression was reduced in the substantia nigra of sporadic PD patients compared to healthy human brains,[20] suggesting potential cross-species conservation of the mechanisms for neurodegeneration. In addition, propionyl-CoA could be generated from α-ketobutyrate. The downregulation of *cth-1*, *cth-2*, and *cbl-1*, which code for cystathionine lyases that convert cystathionine to α-ketobutyrate, and of *cbs-1*, which codes for a cystathionine β-synthase that converts homocysteine to cystathionine, may further reduce the propionyl-CoA level in PD animals (Figure 2D). Since homocysteine can be converted to cystathionine, the reduced *cbs-1*, *cbl-1*, *cth-1*, and *cth-2* levels may lead to increased amounts of homocysteine. In fact, we found increased levels of homocysteine in PD animals compared to the WT animals (Figure S2D), which is consistent with the elevation of homocysteine levels in PD patients compared to heathy individuals.[21]

Besides regulating propionate metabolism, vitamin B_{12} serves as the coenzyme for 5-methyltetrahydrofolate-homocysteine methyltransferase (METR-1) and functions to accelerate the one-carbon cycle. Dietary B_{12} enhances the production of methionine

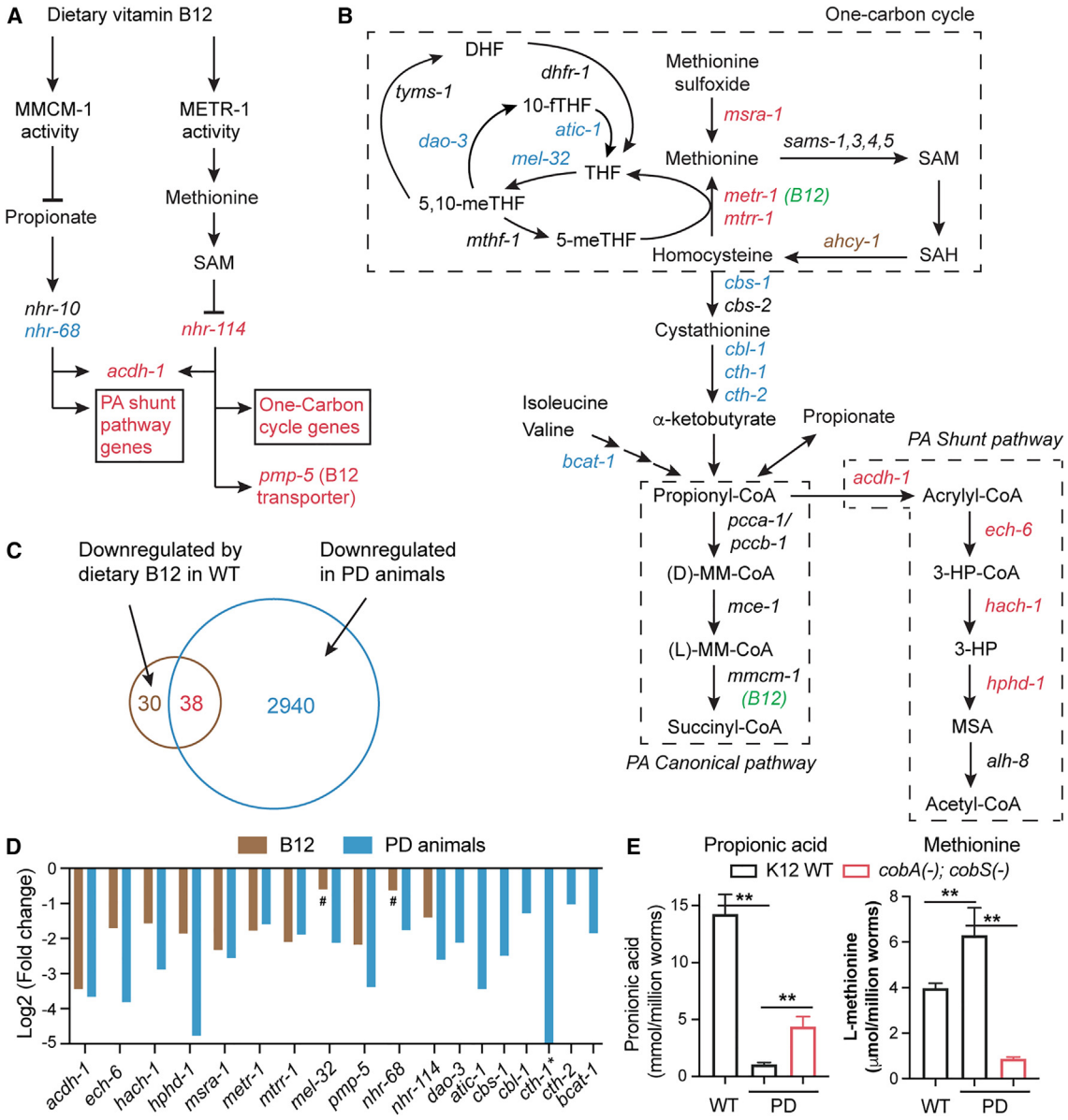

Figure 2. Dietary B_{12} and α-syn aggregation cause similar transcriptional changes

(A) Vitamin B_{12} serves as the coenzyme of methylmalonyl-CoA mutase MMCM-1 and methionine synthase METR-1 to regulate the level of propionate and methionine, respectively, which leads to changes in downstream genes. The pathways are based on works from the Walhout lab.[16–18]

(B) Major enzymes involved in the metabolic network for propionate and methionine are listed. Genes in red are downregulated both in PD animals compared to the WT animals and by dietary B_{12} based on previous studies.[17,18] Genes in brown are only downregulated by B_{12} but not in PD, and genes in blue are only downregulated in PD but not by B_{12}.

(C) Venn diagram showing the overlap of genes downregulated by B_{12} and in PD.

(D) Fold change of genes downregulated by B_{12} and in PD. # indicates that the gene is downregulated but the adjusted p >0.05; Log2 (fold change) for *cth-1* is −5.7, exceeding the limit of the axis.

(E) The level of PA and methionine determined by GC-MS in WT and PD animals fed with different bacteria. Three biological replicates were performed. Double asterisks indicate p < 0.01 in a post-ANOVA Tukey's test.

and SAM, which then suppressed the expression of *acdh-1* and the one-carbon cycle genes, including *metr-1*, *mtrr-1*, *ahcy-1*, *mel-32*, and *mthf-1*.[16] Three of them and two more genes (*dao-3*, and *atic-1*) in the one-carbon cycle were downregulated in PD animals compared to the WT animals. Moreover, both B_{12} and α-syn overexpression repressed *pmp-5* (the B_{12} transporter), *msra-1* (the influx regulator of the one-carbon cycle), and *nhr-114* (the transcription factor that activates the one-carbon cycle genes). Downregulation of the one-carbon cycle genes in PD animals could be caused by increased levels of methionine, since

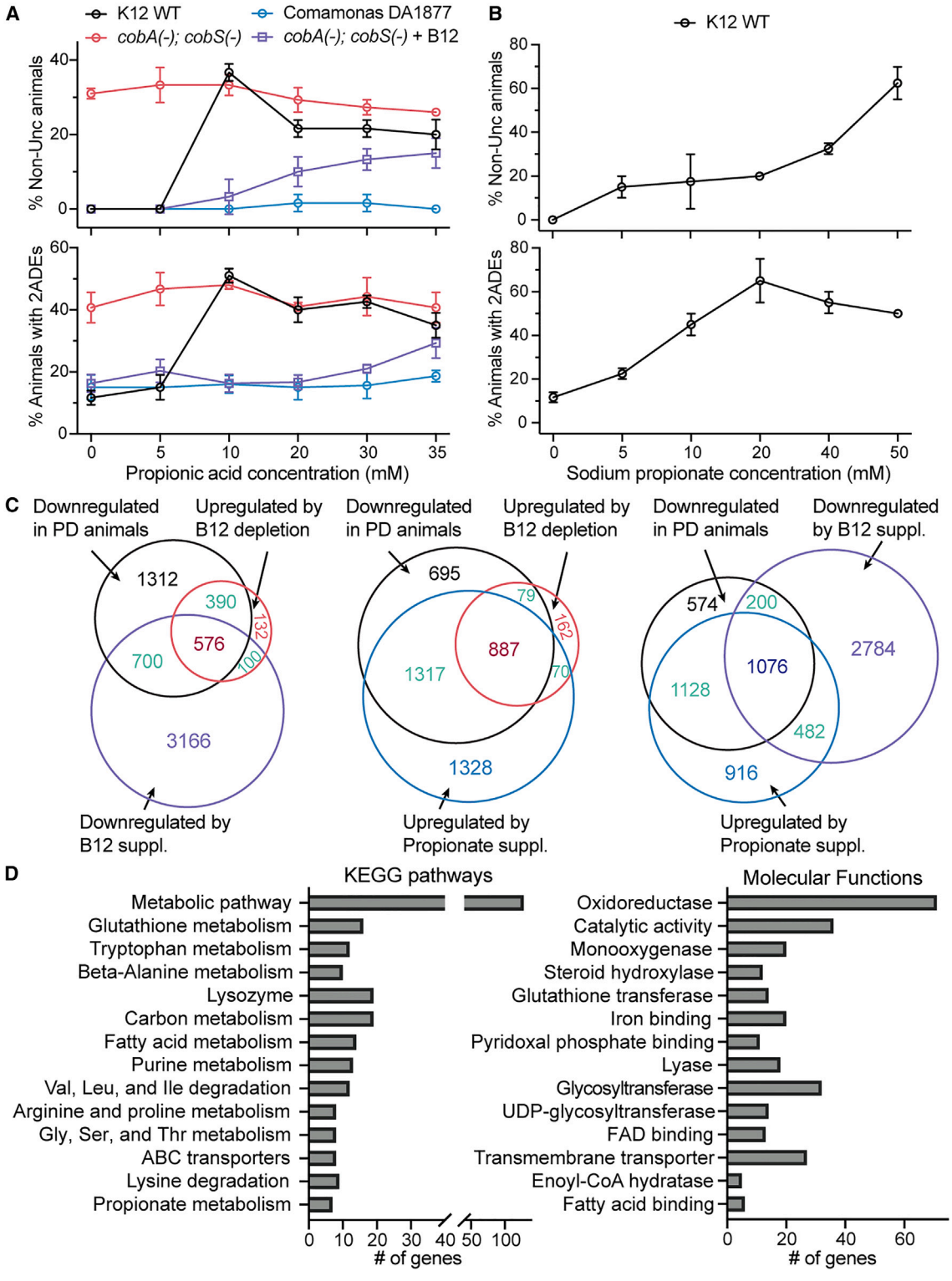

Figure 3. Propionate supplementation suppresses neurodegeneration and corrects PD-associated transcriptomic aberration

(A and B) The percentage of animals with normal locomotion and with 2 intact ADE neurons fed with different bacteria and supplemented with different concentrations of PA or SP (under K12 WT diet).

(legend continued on next page)

methionine supplementation is known to repress these genes.[16] We found that the methionine level was increased in PD animals compared to the WT animals, and it was significantly reduced when dietary B_{12} was depleted (Figure 2E).

Overall, the above results suggest that both excessive dietary B_{12} and neuronal α-syn aggregation in the PD animals lead to similar metabolic changes and transcriptional reprogramming, which may contribute to neurodegeneration. Removing dietary B_{12} can at least partially reverse such metabolic dysregulation in PD animals and rescue neurodegeneration.

Propionate protects neurons from degeneration

We next asked whether decreased propionate or increased methionine abundance mediated the effects of vitamin B_{12} on neurodegeneration. We supplemented PA to the PD animals fed with WT *E. coli* and found that low concentrations of PA (10 mM) significantly suppressed the neurodegenerative phenotypes (Figure 3A). Higher concentrations delayed development and reduced the viability of the PD animals and had a lesser effect on neuroprotection (Figure S3A). Previous studies also found that PA at >40 mM concentration caused slow growth and lethality in WT animals.[18,22] We suspected that the toxicity may result from the acidification when a high concentration of PA was supplemented. In fact, when 35 mM PA was added, the pH of the nematode growth media (NGM) plate dropped from 6.0 to 3.9. This toxicity could be avoided by supplementing sodium propionate (SP), which suppressed neurodegeneration in a dose-dependent manner without lowering pH or affecting viability (Figure 3B).

Importantly, adding propionate did not provide further neuroprotection to the PD animals fed with the *cobS(−); cobA(−) E. coli* mutants, suggesting that eliminating B_{12} from the diet suppressed neurodegeneration through the elevation of propionate levels (Figure 3A). As expected, dietary supplementation of B_{12} or feeding with B_{12}-rich *Comamonas* strongly suppressed the neuroprotective effects of propionate; weak or no protection was observed even at high concentrations of PA (Figure 3A). Thus, vitamin B_{12} likely promotes neurodegeneration by breaking down propionate through the activation of the canonical pathway.

We then supplemented the PD animals with methionine and found that methionine also protected neurons from α-syn-induced degeneration at a high concentration (20 mM; Figure S3B). This neuroprotective effect of methionine is consistent with previous reports in other models of neurodegenerative diseases.[23] Although the PD animals have elevated levels of methionine compared to the WT animals (Figure 2E), the level may not be high enough to trigger neuroprotection. Moreover, methionine supplementation to animals fed with the B_{12}-deficient *cobS(−); cobA(−) E. coli*, which had significantly reduced methionine levels, did not show any detrimental effects (Figure S3B). These results indicated that B_{12}-induced accumulation of methionine in PD animals did not contribute to neurodegeneration. Instead, the B_{12}-induced downregulation of propionate plays the critical role in promoting neurodegeneration.

B_{12} depletion or propionate supplementation reverses PD-associated transcriptomic aberration

The level of propionate appeared to dictate the expression of a large number of genes associated with PD pathogenesis in the *C. elegans* model. Through transcriptomic profiling, we found that among the 2,978 genes downregulated in PD animals compared to the WT animals, the expression of 966 genes were restored by feeding the PD animals with B_{12}-deficient *E. coli*, and the majority (576) of them were resuppressed by supplementing B_{12} in the *cobA(−); cobS(−) E. coli* diet (Figure 3C; Tables S1, S2, and S3). Interestingly, B_{12} supplementation caused the suppression of approximately half (1,276) of the 2,978 genes that were downregulated in PD animals, which supported the idea that B_{12} and α-syn aggregation target the same set of genes.

Moreover, 887 (92%) of the above 966 genes upregulated by dietary B_{12} depletion were also upregulated upon propionate supplementation, confirming that the neuroprotective effects of removing B_{12} from the diet was mediated mainly by increased propionate levels (Figure 3C; Table S4). Strikingly, propionate supplementation upregulated 2,204 (74%) of the 2,978 genes downregulated in PD. Similar trends were also observed for the 2,988 genes upregulated in PD, 2,665 genes (89%) of which were downregulated by propionate supplementation (Figure S3C). These results suggest that a large majority of the transcriptomic changes associated with PD pathology in *C. elegans* could be reversed by simply restoring the propionate levels.

Although B_{12} depletion only partially restored the propionate level to ~30% of the physiological levels found in the WT animals (Figure 2E), this moderate increase in propionate abundance had significant effects on the transcriptome by restoring the normal expression of a key set of PD genes. In fact, when we supplemented propionate to animals already fed with a B_{12}-deficient diet, very few PD genes showed statistically significant changes in expression (Figure S3D; Table S5), suggesting that increasing propionate levels further may not produce stronger antineurodegenerative effects. This observation is consistent with the similar penetrance of the degenerative phenotypes in animals that were fed with a B_{12}-deficient diet or supplemented with propionate (Figure 3A). Nevertheless, propionate supplementation appeared to affect the expression of more genes than B_{12} depletion, suggesting that certain genes may only respond to high levels of propionate.

Next, we focused on the 887 PD-downregulated genes that were upregulated by both B_{12} depletion and propionate supplementation. This set of genes included the propionate shunt pathway genes (*acdh-1*, *ech-6*, *hach-1*, and *hphd-1*) that were known to be regulated by propionate.[17] Gene Ontology (GO) analysis found enrichment of genes involved in fatty acid and amino acid metabolisms, as well as enzymatic activities associated

(C) Venn diagrams showing the overlapping of genes differentially expressed in PD animals compared to the WT animals, affected by the B_{12}-deficent *cobA(−); cobS(−)* diet, and regulated by the supplementation of 60 nM B_{12} or 10 mM PA.

(D) Enriched GO terms based on DAVID analysis of the 887 PD-downregulated genes that were upregulated by both B_{12} depletion and propionate supplementation. For all enriched GO terms, $p < 0.05$ in Fisher's exact test.

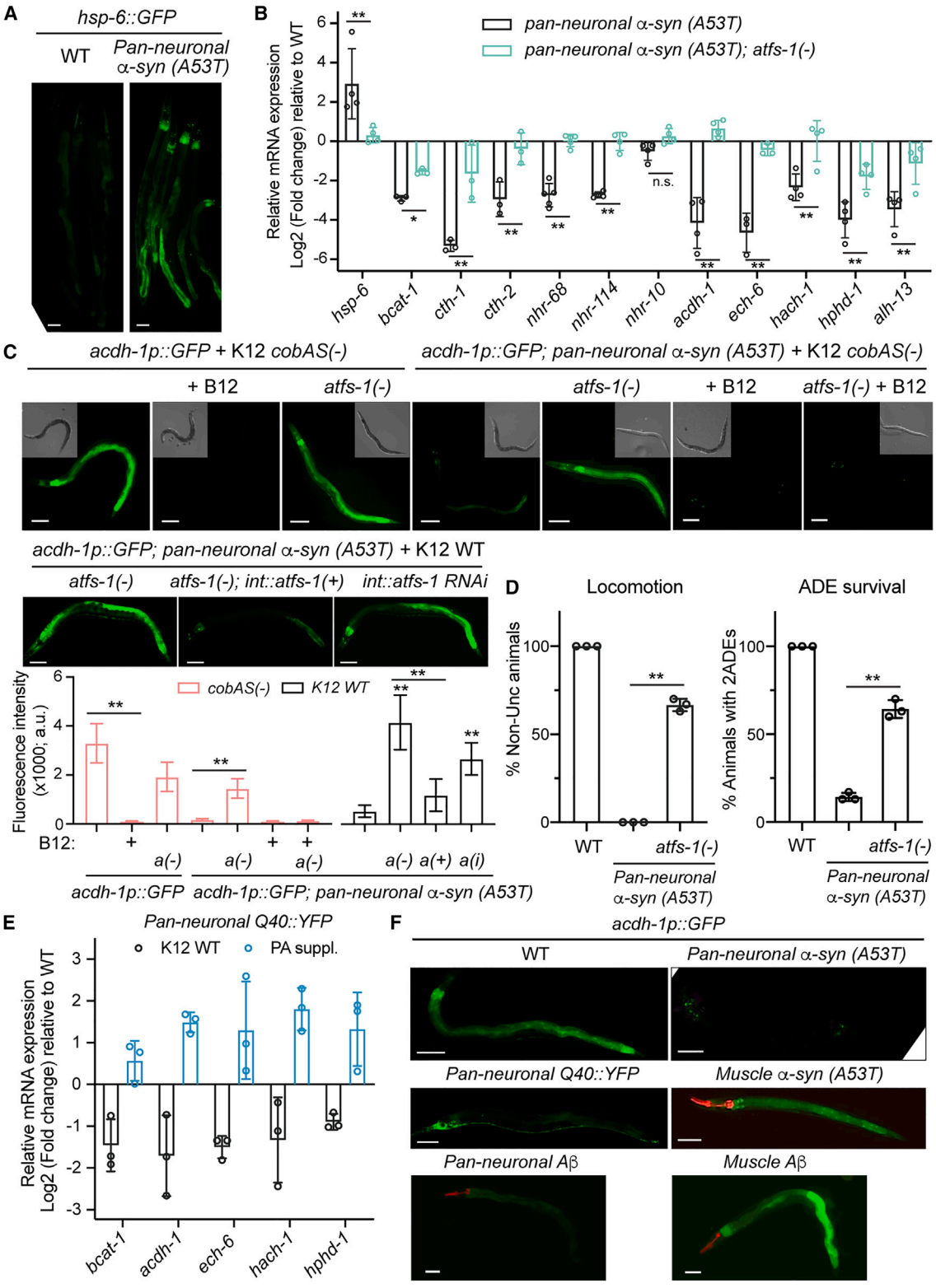

(legend on next page)

with metabolism (Figure 3D). Therefore, the abundance of propionate serves as a signal to activate metabolic genes that promote lipid and amino acid metabolism and energy production.

Neuronal α-syn activates intestinal mitoUPR and changes intestinal gene expression

One intriguing finding of our transcriptomic studies was that many of the downregulated genes in the PD animals were expressed mainly in the intestine. Using the available single-cell RNA sequencing (RNA-seq) data,[24] we found that 101 of the above 887 B_{12}- and propionate-sensitive PD-downregulated genes had strong intestinal expression (transcripts per million [TPM] >100) and weak or no neuronal expression (average TPM across neuron types <20). Using *acdh-1* as an example, we constructed an *acdh-1p::GFP::H2B* reporter and found that its expression was observed mainly in the intestine and hypodermis and had no overlapping with a pan-neuronal marker (Figure S4A), suggesting that *acdh-1* was not expressed in the nervous system and that its downregulation in the PD animals was probably due to cell-non-autonomous effects.

How could neuronal α-syn lead to transcriptomic changes in the intestine? Previous studies found that protein aggregation-induced mitochondrial stress in neurons could trigger mitoUPR in the intestine through secreted signaling molecules.[25] Neuronal α-syn overexpression induced the activation of mitoUPR marker *hsp-6* in the intestine (Figure 4A). To test whether mitoUPR triggered the downregulation of intestinal genes in the PD animals, we deleted the stress-activated transcription factor *atfs-1*, which is responsible for activating mitoUPR.[26] Reverse-transcription quantitative real-time PCR (RT-qPCR) revealed that the downregulation of many metabolic genes, including the propionate-producing genes (e.g., *bcat-1*, *cth-1*, *cth-2*) and the propionate-responsive genes (e.g., *nhr-68*, *acdh-1*, *ech-6*, *hach-1*, *hphd-1*) were abrogated in PD animals carrying mutations in *atfs-1* (Figure 4B).

Moreover, using the *acdh-1p::GFP* fluorescent reporter, we confirmed the downregulation of *acdh-1* expression in the intestine by neuronal α-syn and that this downregulation depended on the mitoUPR activator ATFS-1 (Figure 4C). Intestine-specific knockdown of *atfs-1* derepressed *acdh-1*, whereas intestine-specific rescue of *atfs-1* in the *atfs-1(−)* mutants restored the repression of *acdh-1* in PD animals, supporting the fact that *atfs-1* functions in the intestine. These results suggest that the activation of intestinal mitoUPR is required for the metabolic disruption that reduces propionate levels, which subsequently cause transcriptomic changes in the intestine. Consistent with this idea, the deletion of *atfs-1* not only blocked mitoUPR but also suppressed α-syn-induced neurodegeneration (Figure 4D). Interestingly, previous work found that the overexpression of gain-of-function ATFS-1 induced DA neuron death,[27] supporting a proneurodegenerative role for sustained mitoUPR. Nevertheless, B_{12} supplementation repressed *acdh-1* expression regardless of ATFS-1, because B_{12} could induce propionate breakdown through the canonical pathways independent of mitoUPR (Figure 4C).

Cell-non-autonomous mitoUPR relies on the mitokines (e.g., serotonin, Wnt) released by neurons that are under proteotoxic stress.[25] We found that deleting *tph-1*, which codes for the tryptophan hydroxylase required for serotonin synthesis, or *egl-20*, which codes for a Wnt ligand, blocked the repression of *acdh-1p::GFP* by neuronal α-syn (Figure S4B), supporting that neuronal proteotoxicity regulates intestinal metabolic genes through cell-non-autonomous mitoUPR pathways.

We further confirmed the neuron-to-intestine signaling using other models of neuronal protein aggregation. Pan-neuronal expression of polyglutamine (Q40) fused with yellow fluorescent protein (YFP) led to similar downregulation of propionate-producing genes and propionate-responsive genes (Figure 4E) and repression of *acdh-1p::GFP* in the intestine as α-syn did (Figures 4E and 4F). Pan-neuronal Aβ1-42 also repressed intestinal *acdh-1* expression (Figure 4F). Even DA neuron-specific expression of α-syn was able to activate mitoUPR marker, repress *acdh-1p::GFP*, and cause similar transcriptomic changes in the intestine, although to a lesser extent than pan-neuronal α-syn (Figure S5; Table S6). Importantly, this interorgan regulation is restricted to the nervous system because muscle expression of either α-syn or Aβ could not repress *acdh-1p::GFP* in the intestine (Figure 4F). These results are expected, since protein aggregation in the muscle does not induce intestinal mitoUPR[25] and thus would not alter propionate metabolism and the expression of propionate downstream genes. It is worth noting that recent studies using *C. elegans* AD models with muscle expression of Aβ found that vitamin B_{12} could alleviate Aβ-induced proteotoxicity.[28,29] This discrepancy with our results may be explained by the distinct effects of neuronal and muscle protein aggregation on intestinal mitoUPR.

Enhancing intestinal production of propionate suppresses α-syn-induced neurodegeneration

The above results suggested that neuronal α-syn accumulation triggered intestinal mitoUPR, which caused the downregulation

Figure 4. Neuronal α-syn aggregation induces intestinal mitoUPR and metabolic rewiring

(A) Activation of the mitoUPR marker *hsp-6p::GFP* in the intestine of PD animals with pan-neuronal α-syn. Scale bars, 100 μm (also in C and F).

(B) Log2-transformed fold change of expression (measured by RT-qPCR) of various genes in PD animals and *atfs-1(gk3094)* PD animals compared to WT animals. All were fed with K12 WT bacteria. Single and double asterisks indicate $p < 0.05$ and $p < 0.01$ in a corrected t test, respectively.

(C) Intestinal expression of *acdh-1p::GFP* in WT animals, *atfs-1(gk3094)* mutants, PD animals, and *atfs-1(−)* PD animals with or without 60 nM B_{12} supplementation, as well as PD animals with intestine-specific *atfs-1* knockdown or intestine-specific *atfs-1* rescue in the *atfs-1(−)* background. Fluorescent intensity of the whole animal was quantified ($N \geq 20$); *a*, *afts-1*.

(D) The locomotion and ADE survival in *atfs-1(gk3094)* PD animals fed with *E. coli* K12 WT bacteria. $N \geq 30$ for each of 3 replicates. Double asterisks indicate $p < 0.01$ in a post-ANOVA Dunnett's or Tukey's test.

(E) Fold change of expression (by RT-qPCR) in AM101 animals with pan-neuronal Q40::YFP compared to the WT animals, and the fold change caused by 10 mM PA.

(F) Expression of *acdh-1p::GFP* in animals with either pan-neuronal (from *rab-3* promoter) or body wall muscle expression (from *myo-3* promoter) of α-syn (A53T) or Aβ1-42.

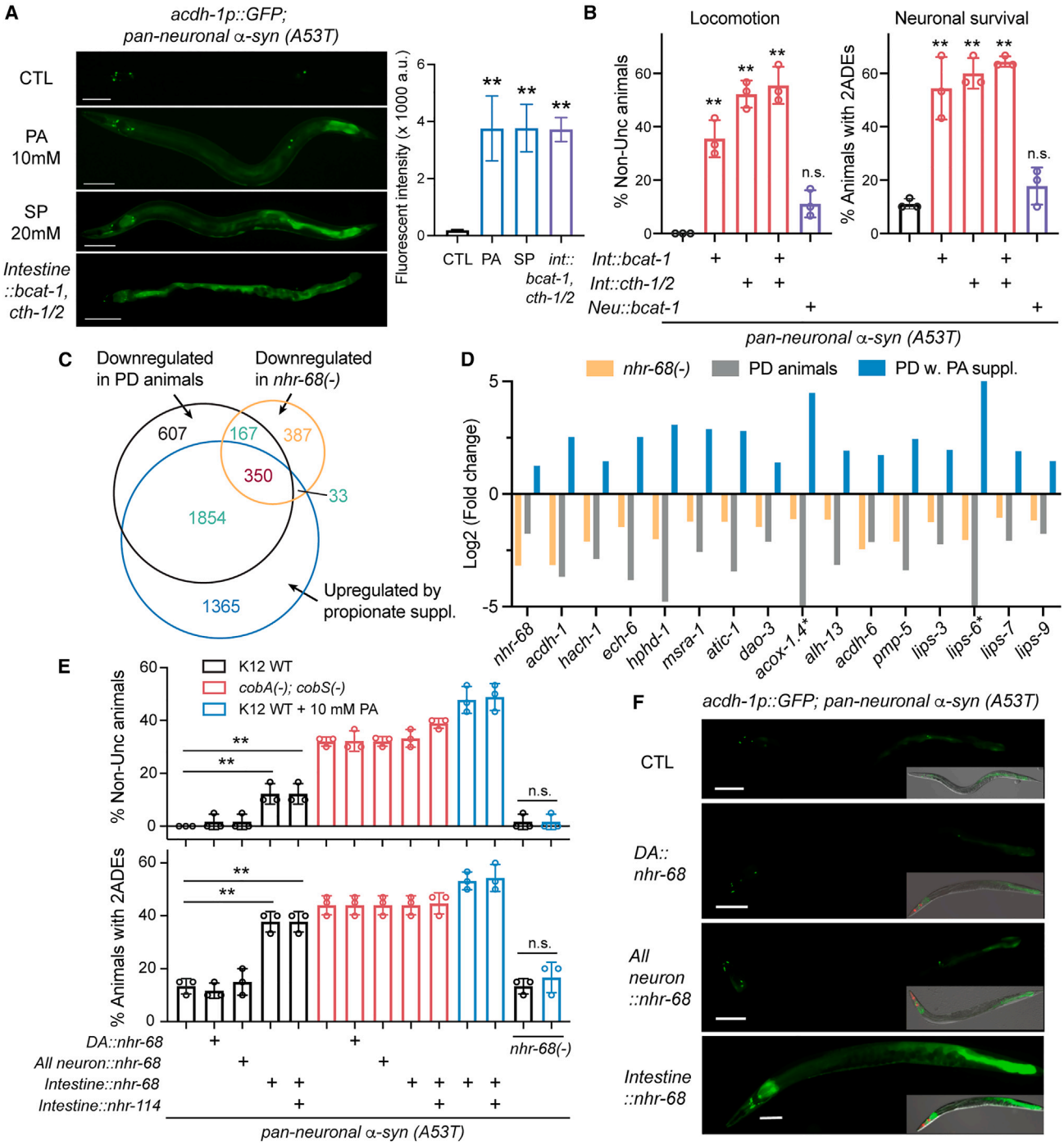

Figure 5. Restoring propionate production or *nhr-68* expression in the intestine rescues neurodegeneration

(A) The expression of *acdh-1p::GFP* in the PD animals with PA or SP supplementation or intestinal overexpression of *bcat-1*, *cth-1*, and *cth-2*. Scale bars, 100 μm. Fluorescent intensity was quantified based on >20 animals.

(B) Locomotion and ADE survival in PD animals (N ≥ 30 in each replicate), with intestine-specific expression of *bcat-1* or *cth-1* and *cth-2* or both or pan-neuronal expression of *bcat-1*.

(C) Venn diagram showing the overlap of genes downregulated in PD animals with genes regulated by *nhr-68* and propionate.

(D) Log2-transformed fold change of expression in *nhr-68(gk708)* mutants and PD animals compared to WT animals and in PD animals with or without propionate treatment. Data were derived from statistically significant RNA-seq results. Log2 (fold change) for *acox-1.4* in PD is −5.4 and for *lips-6* is −5.8 in PD and 5.8 by PA treatment.

(legend continued on next page)

of genes involved in propionate production. Reduced propionate levels then resulted in transcriptomic reprogramming in the intestine, which in turn promoted neurodegeneration. Supporting this hypothesis, supplementation of either PA or SP could restore the intestinal expression of propionate-sensitive genes, such as *acdh-1p::GFP* (Figure 5A), and rescue α-*syn*-induced neurodegeneration (Figures 3A and 3B).

In addition to dietary supplementation, genetic enhancement of propionate production in the intestine suppressed neurodegeneration. Since the reduction of propionate levels may be caused by the downregulation of *bcat-1*, *cth-1*, and *cth-2*, which promote the conversion of either BCAA or cystathionine into propionyl-CoA (Figure 2B), we overexpressed these genes either individually or in combination from the intestine-specific *ges-1* promoter and found significant rescue of locomotion defects and DA neuron death (Figure 5B). As expected, the expression of the propionate-responsive *acdh-1p::GFP* was significantly increased by intestinal expression of *bcat-1*, *cth-1*, and *cth-2*, supporting the increase in propionate level (Figure 5A). These results indicate that restoring propionate production in the intestine could inhibit α-syn-induced neurotoxicity. In contrast, the overexpression of *bcat-1* from the pan-neuronal *rab-3* promoter had little effect, suggesting that the intestine is likely to be the major site of propionate production (Figure 5B).

Restoring intestinal expression of propionate-responsive genes rescues neurodegeneration

How does propionate suppress neurodegeneration? Because moderate increases in the propionate level upon the depletion of dietary B_{12} had significant rescuing effects on neurodegeneration, and propionate supplementation changed the expression of thousands of genes, we reasoned that propionate likely served as a key signaling molecule to control metabolic networks. Using *acdh-1* as an example of propionate downstream genes, we searched for the transcription factors that control the propionate-responsive genetic program. Previous work identified three nuclear hormone receptors as the regulators of *acdh-1* expression, including *nhr-10* and *nhr-68* mediating propionate-induced activation and *nhr-114* mediating methionine-induced repression (Figure 2A).[16,30] Among the three genes, *nhr-68* and *nhr-114* were downregulated in PD animals and upregulated by propionate supplementation. The finding that *nhr-114* was propionate responsive in the PD animals supports the possible crosstalk between the propionate-dependent and Met/SAM-dependent pathways downstream of B_{12}.[16]

We next focused on the potential role of *nhr-68* as the master regulator that mediates the effects of propionate on downstream genes. Among the 943 genes (compiled from previous studies;[30] Table S7) regulated by *nhr-68*, 517 were significantly downregulated in PD animals, and the majority (350) of them were upregulated by propionate supplementation, including *acdh-1*, *hach-1*, *ech-6*, and *hphd-1*, as well as other genes involved in lipid and amino acid metabolism (Figures 5C and 5D). These transcriptomic data support that the downregulation of *nhr-68* by decreased propionate could result in the repression of many downstream metabolic genes. To test whether restoring their expression could protect neurons from degeneration, we overexpressed *nhr-68* in the PD animals using tissue-specific promoters. Intestine-specific expression of *nhr-68* activated *acdh-1p::GFP* and suppressed neurodegenerative phenotypes, whereas DA neuron-specific or pan-neuronal expression of *nhr-68* had little effect (Figures 5E and 5F). These results indicated that *nhr-68* and its downstream module function in the intestine to exert neuroprotective effects. Importantly, in *nhr-68(−)* PD animals, propionate supplementation did not show any anti-degenerative effects (Figure 5E), supporting that propionate acts through *nhr-68* to regulate downstream genes and to modulate neurodegeneration.

Nevertheless, depleting dietary B_{12} or supplementing propionate led to additional neuroprotection in animals that had restored intestinal *nhr-68* expression. Therefore, *nhr-68* is not the only transcription factor downstream of propionate, which is somewhat expected given that a large fraction (1,854 out of 2,204 [84%]) of propionate-induced PD genes are not regulated by *nhr-68* (Figure 5C). The overexpression of both *nhr-68* and *nhr-114* had the same effects as expressing *nhr-68* alone, suggesting that they act in the same pathway (Figure 5E). Thus, propionate likely activates multiple transcription factors (with *nhr-68* being a major one), which then regulate a myriad of downstream metabolic genes.

Propionate promotes mitochondrial function, cellular respiration, and energy production

The propionate-upregulated PD genes included not only the propionate shunt pathway genes but also many genes that are involved in fatty acid oxidation and amino acid degradation, the products of which were fed into the tricarboxylic acid cycle to generate energy. For example, propionate activates the expression of acyl-CoA dehydrogenases *acdh-1*, *-6*, *-9*, *-10*, *-11*, and *-12*; acyl-CoA oxidases *acox-1.1, -1.2, -1.3*, *-1.4*, and *-1.6*; acetyl-CoA acetyltransferases *kat-1* and *T02G5.7*; 3-ketoacyl-CoA thiolases *acaa-2* and *hadb-1*; enoyl-CoA hydratases *ech-1.1*, *-1.2*, *-4*, *-5*, *-6*, *-7*, and *-8*; lipases *lips-3*, *-6*, *-7*, *-9*, and *-10*; aconitate hydratase *aco-1*; isocitrate dehydrogenase *idh-1*; succinate dehydrogenase *sdha-1*; and succinate-CoA ligases *suca-1* and *sucl-1*, and so forth. Moreover, at least 85 propionate-responsive genes encode proteins that function in the mitochondria. Thus, we hypothesize that propionate may signal to promote mitochondrial functions and energy production in the intestine. To test this idea, we measured the aerobic respiration rate of PD animals using the Seahorse XF analyzer. Compared to the WT animals, PD animals showed a much lower ATP-linked respiration rate, which can be significantly rescued by depleting dietary B_{12} or supplementing propionate

(E) Locomotion and ADE survival in PD animals (N ≥ 30) overexpressing *nhr-68* in DA neurons, all neurons, or the intestine and *nhr-68(−)* PD animals under various conditions.

(F) The expression of *acdh-1p::GFP* in PD animals that expressed *nhr-68* in neurons or intestine. Double asterisks indicate $p < 0.01$ in a post-ANOVA Dunnett's or Tukey's test. Scale bars, 100 μm.

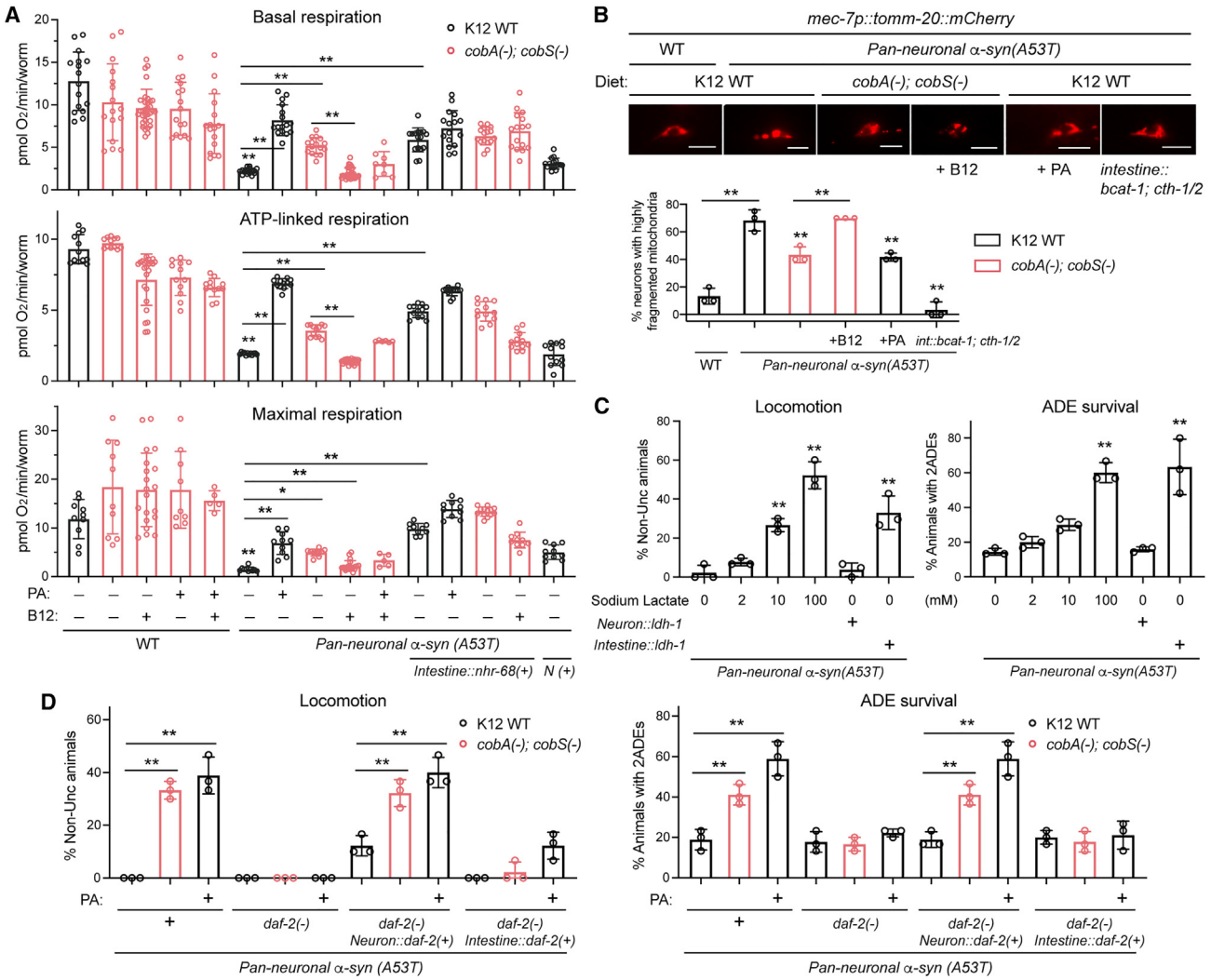

Figure 6. Propionate regulates intestinal energy production and confers neuroprotection through intestine-neuron signaling

(A) Basal respiration, ATP-linked respiration, and maximal respiration (measured as oxygen consumption rate) of day 1 adults of WT and PD animals fed with WT or B_{12}-deficient K12 bacteria. Conditions for 10 mM PA or 60 nM B_{12} supplementation and intestinal or neuronal [*N (+)*] overexpression of *nhr-68* were also included. Results of 12–24 repeats were shown as mean ± SD.

(B) Mitochondrial morphology in ALM neurons (visualized by *mec-7p::tomm-20::mCherry*) of PD animals fed with WT or B_{12}-deficient K12 bacteria and supplemented with B_{12} or PA. Scale bars, 10 μm. The percentage of neurons with fragmented mitochondria was quantified (N ≥ 30 in each replicate).

(C) Locomotion and ADE survival of PD animals (N ≥ 30) supplemented with different concentrations of sodium lactate and in animals with pan-neuronal or intestinal overexpression of *ldh-1*.

(D) Locomotion and ADE survival of PD animals (N ≥ 30) with *daf-2(e1370)* mutations and *daf-2(−)* PD animals with neuron- or intestine-specific rescue; animals were fed with either WT or B_{12}-deficient K12. Single and double asterisks indicate $p < 0.05$ and $p < 0.01$, respectively, in a post-ANOVA Dunnett's or Tukey's test compared with the WT or between specific pairs.

(Figure 6A). As expected, B_{12} supplementation countered the effects of propionate and suppressed cellular respiration.

Importantly, intestine-specific restoration of *nhr-68* expression rescued the ATP-linked respiration in PD animals, whereas pan-neuronal expression of *nhr-68* failed to do so. Furthermore, B_{12} depletion or propionate supplementation had weak effects on the oxygen consumption rate in PD animals that overexpressed *nhr-68*, which is consistent with the idea that propionate acts through *nhr-68* (Figure 6A). Basal and maximal respiration rates followed the trend of mitochondrial respiration, whereas non-mitochondrial respiration showed little difference among the treatments (Figure S6A). These results support that propionate boosts mitochondrial functions in the PD animals by activating downstream metabolic genes.

Enhanced mitochondrial functions in the intestine appeared to also improve mitochondrial health in neurons. Using a mitochondrial marker *tomm-20::mCherry* expressed in the touch receptor neurons, we found that the α-syn-induced fragmentation of neuronal mitochondria could be rescued by removing dietary B_{12} or supplementing propionate or intestine-specific

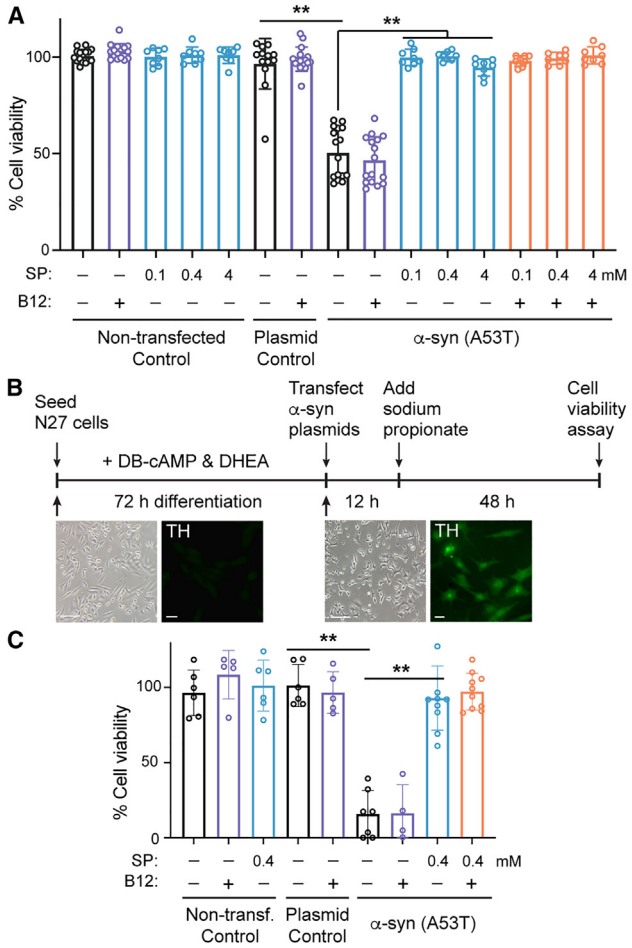

Figure 7. Propionate shows neuroprotective effects in mammalian neurons

(A) Representative results of cell viability assays using the human neuroblastoma SH-SY5Y cells transfected with α-syn (A53T)-expressing constructs and treated with 5 μM B_{12} or the indicated concentrations of SP or both. Transfection with empty vectors was used as plasmid controls. Mean ± SD is shown.

(B) The experimental scheme for the rat N27 DA neural cells. The differentiation process caused morphological changes and the expression of tyrosine hydroxylase (detected by immunofluorescence) of N27 cells. The bright-field and fluorescent images were taken at different magnifications (scale bars, 100 and 20 μm, respectively).

(C) Representative results of cell viability assay using differentiated N27 cells that expressed α-syn (A53T) and were treated with 0.4 mM SP, according to the scheme in (B). Double asterisks indicate $p < 0.01$ in a post-ANOVA Tukey's test.

overexpression of propionate-producing genes (Figure 6B). Since propionate mostly activates metabolic genes in the intestine, we reason that the increase in intestinal energy production may suppress neurodegeneration by improving neuronal mitochondrial functions through intestine-to-neuron signaling. Supporting this hypothesis, we found that both B_{12} depletion and propionate supplementation reduced intestinal mitoUPR presumably by relieving mitochondrial stress in neurons (Figure S6B). Thus, our results suggest a potential positive feedback loop for the neuroprotective effects of propionate. Increased propionate accelerates cellular respiration and energy metabolism in the intestine, which cell non-autonomously improves neuronal mitochondrial health, which in turn reduces the activation of mitoUPR in the intestine, leading to further increase in propionate production. Interestingly, propionate did not alleviate cell-autonomous mitoUPR in the intestine induced by feeding RNAi against *cco-1* (Figure S6C),[25,31] suggesting a specific role for propionate in the interorgan regulations between intestine and neurons.

How does the metabolic state of intestine affect neuronal health? Inspired by the lactate-mediated metabolic coupling between glia and neuron in mammals,[32] we tested whether lactate plays a role in neurodegeneration. The supplementation of sodium lactate to PD animals suppressed neurodegenerative phenotypes in a dose-dependent manner, and intestine-specific overexpression of the lactate dehydrogenase *ldh-1* (which was downregulated in PD animals) had similar effects (Figure 6C), suggesting the possibility of intestine-provided lactate serving as an energy substrate for neurons in *C. elegans*. Moreover, some known intestine-to-neuron signaling involved insulin-like peptides,[33] so we tested whether the propionate-mediated neuroprotection required the insulin signaling by removing the sole insulin receptor DAF-2. Indeed, the *daf-2(–)* PD animals were insensitive to either propionate supplementation or the depletion of dietary B_{12} (Figure 6D). Importantly, neuron-specific rescue of *daf-2* restored the sensitivity to propionate, indicating that DAF-2 functions in neurons to receive the signals from intestine-released insulin-like peptides, which could mediate the interorgan communication downstream of propionate.

Propionate protects against α-syn proteotoxicity in mammalian neurons

Finally, we asked whether propionate had direct effects on α-syn-induced proteotoxicity in mammalian neurons. After transfecting human neuroblastoma SH-SY5Y cells with plasmids expressing α-synuclein (A53T), we treated the cells with vitamin B_{12} or SP or both. Strikingly, even low concentrations (100 μM) of SP were able to suppress α-syn-induced cell death (Figure 7A), indicating that the neuroprotective effects of propionate are conserved across species. B_{12} supplementation had no effects on neurodegeneration and could not antagonize the effects of propionate supplementation in human cells. We reason that this is likely because the cell culture medium already contained a large amount of B_{12}. Similar neuroprotective effects of propionate were observed in rat DA neurons that were differentiated from the N27 neural cell line (Figures 7B and 7C). These results suggest that in addition to inhibiting neurodegeneration through interorgan signaling, propionate may directly protect neurons from proteotoxicity.

DISCUSSION

Among the 38 proneurodegenerative *E. coli* genes identified in the genome-wide screen, we previously characterized the genes responsible for producing the bacterial amyloid fibril curli, which could enter the host neurons to cross-seed the aggregation of α-syn and promote neurodegeneration.[14] In this study, we focus on another set of genes that are responsible for synthesizing

vitamin B_{12}. Unlike curli, B_{12} does not affect α-syn aggregation (Figure S1) and modulates neurodegeneration downstream of α-syn by inducing the breakdown of propionate, which is a key activator of metabolic genes involved in fatty acid and amino acid metabolism and energy production. Removing B_{12} or supplementing propionate in the diet could metabolically rescue neurodegeneration without reversing α-syn aggregation, indicating the possibility of treating neurodegenerative diseases by simply changing the level of certain metabolites. The neurodetrimental effect of vitamin B_{12} in *C. elegans* is somewhat surprising since several studies observed B_{12} deficiency in PD patients,[34] and B_{12} supplementation had some beneficial effects, although it did not significantly improve clinical outcomes.[35] We reason that the regulation of SCFAs by B_{12} is likely different in *C. elegans* PD models and PD patients, given that *C. elegans* produces SCFAs by metabolizing amino acids, whereas humans mostly obtain SCFAs from the anaerobic gut bacteria that ferment dietary fibers. In fact, B_{12} appears to increase propionate and butyrate production by the human gut microbiota[36] while also serving as a coenzyme of methylmalonyl-CoA mutase to break down propionate. Thus, the effect of B_{12} on SCFAs and neurodegeneration is more complex in humans than in *C. elegans*. However, the neuroprotective effects of SCFAs are consistent across species.

Our studies and others suggest that SCFAs are promising candidates for the metabolic rescue of PD. Compared to healthy individuals, PD patients have reduced levels of SCFAs, likely due to the significant reduction of *Prevotellaceae* family bacteria that are good at producing SCFAs by fermenting dietary fibers.[37] In the PD *C. elegans*, we also observed lower levels of PA and butyric acid, compared to the healthy controls (Figures 2E and S6A). Supplementation of propionate protected neurons from α-syn-induced neurodegeneration. Although high concentrations ($\geq$40 mM) of PA were considered toxic to *C. elegans* by previous studies,[18] this toxicity likely resulted from the acidification of the culturing medium instead of the abundance of propionate, because the same concentration (e.g., 40 or 50 mM) of SP did not generate any toxicity (Figure S3A). A low concentration (10 mM) of PA showed strong neuroprotection without causing lethality. In addition to propionate, sodium butyrate suppressed neurodegenerative phenotypes in a dose-dependent manner (Figures S6D and S6E), supporting the beneficial effects of SCFAs in *C. elegans* PD models. Our results in *C. elegans* are consistent with the findings in cellular and mouse models of PD. For example, PA increased the survival of mouse primary DA neurons against rotenone-induced toxicity,[8] and we found that SP protected human neuroblastoma cells and rat DA neurons against α-syn proteotoxicity. Similarly, butyric acid rescued α-syn overexpression-induced DNA damage in Lund human mesencephalic cells.[38] In mouse PD models, oral supplementation of propionate and butyrate also protected neurons from chemically induced degeneration and ameliorated motor impairments.[7,9] Thus, the protective effects of SCFAs appear to be conserved across multiple models in different species.

One surprising finding in this study is the cell-non-autonomous effects of SCFAs. First, the lower level of propionate in PD animals is caused by neuron-to-intestine signaling, which triggers intestinal mitoUPR and transcriptomic changes that lead to the downregulation of propionate-producing genes. Then, the reduced abundance of propionate represses a network of metabolic genes and causes energy failure in the intestine, which then exacerbates neurodegeneration through intestine-to-neuron signaling. Propionate supplementation or the overexpression of key metabolic regulators restores the energy metabolism in the intestine, which leads to better neuroprotection possibly through intestine-derived energy substrate (e.g., lactate) and signaling molecules (e.g., insulin-like peptides). Overall, our results provide *in vivo* evidence to support a critical role for SCFAs in the gut-brain axis in neurodegenerative diseases. In humans, SCFAs produced by the gut microbes may also modulate neurodegeneration through cell-non-autonomous mechanisms, such as by regulating intestinal epithelial cells, gut barrier function, and systematic inflammation.[39–41]

What are the molecular targets of SCFAs? Propionate can bind and activate mammalian G protein-coupled receptors (GPCRs) expressed on intestinal epithelial cells and immune cells.[41,42] Given that *C. elegans* has over 1,000 GPCRs,[43] it is entirely possible that propionate can activate cellular signaling by binding to GPCRs. Activation of the GPCR signaling may induce the expression of *nhr-68*, which is a key transcriptional regulator downstream of propionate. Moreover, propionate and butyrate are inhibitors of histone deacetylase.[44,45] Therefore, they may reshape the transcriptional landscape by modulating histone modifications. The fact that propionate altered the expression of thousands of genes in the PD animals supports its role in reprogramming the transcriptome. Moreover, we found that propionate-induced transcriptional changes boost mitochondrial functions and ATP-linked respiration, which is consistent with a recent report that propionate improved mitochondrial respiration and morphology in regulatory T cells (Tregs), leading to better Treg differentiation and reduced inflammation.[46] Therefore, SCFAs may exert their activities through multifaceted mechanisms.

Limitations of the study

A major challenge in understanding the mechanism underlying the neuroprotective effects of SCFAs is to disentangle their direct effects on neurons from their indirect effects through other cells. In this study, we supplemented the PD *C. elegans* with propionate, which can act on both neurons and non-neuronal tissues. Although we showed that propionate upregulated intestinal genes and suppressed neurodegeneration through the interorgan signaling between intestine and neurons, we could not rule out any direct effects of propionate on neurons. In fact, propionate modulates the expression of thousands of genes, many of which are expressed exclusively in neurons. The change in their expression could result from either the direct effect of propionate on neurons or indirect regulation through the intestine-derived metabolites and signaling molecules. Similar challenges exist in mammalian PD models in which SCFAs have been shown to directly prevent neuronal death in cell culture[8] (also this study) and indirectly influence neuronal health by regulating intestinal epithelial cells, glia, and immune cells.[39,41,46] One potential way to differentiate the neuron-autonomous and non-autonomous effects would be to identify the molecular targets of propionate,

manipulate their expression in specific tissues, and then assess the therapeutic outcome of propionate supplementation.

Moreover, for the cell-non-autonomous regulation, considerable efforts will be needed to understand how the non-neuronal cells influence the metabolism, physiology, and survival of neurons. Although our results hinted that lactate and insulin-like peptides derived from intestinal cells may modulate neuronal health, the mechanism is not fully elucidated. Neurodegeneration is likely regulated by a diverse array of secreted molecules derived from non-neuronal tissues.

Lastly, our work uncovered an unexpected detrimental effect of vitamin B_{12} on neurodegeneration. It is unclear whether this effect is specific to the *C. elegans* PD model or can be extrapolated to mammalian systems. Given the complexity in the regulation of propionate metabolism by B_{12} in mammals, further investigation will be needed to understand its true effects on neurodegeneration. For example, since most neuronal cell culture media contain potentially a large amount of B_{12} from the serum, a serum-free cellular PD model is needed to test the role of B_{12}. A longitudinal study in PD mice supplemented with varying doses of vitamin B_{12} can also help understand its net *in vivo* effects on neurodegeneration in mammals.

STAR★METHODS

Detailed methods are provided in the online version of this paper and include the following:

- KEY RESOURCES TABLE
- RESOURCE AVAILABILITY
  - Lead contact
  - Materials availability
  - Data and code availability
- EXPERIMENTAL MODEL AND STUDY PARTICIPANT DETAILS
  - *C. elegans* strains
  - Cell lines and culture conditions
- METHOD DETAILS
  - Constructs, transgenes, and RNAi
  - Construction of double knockout K12 *E. coli* bacteria
  - Immunofluorescence and fluorescent imaging
  - Sequential fractionation and western blot
  - Behavioral assays
  - Mass spectrometry
  - RNA-seq and RT-qPCR
  - Mitochondrial respiration assay
  - Mammalian cell culture and cell viability assay
- QUANTIFICATION AND STATISTICAL ANALYSIS

SUPPLEMENTAL INFORMATION

Supplemental information can be found online at https://doi.org/10.1016/j.celrep.2024.113865.

ACKNOWLEDGMENTS

We thank Prof. Garry Wong at the University of Macau and Prof. Aixin Yan at the University of Hong Kong for providing strains and DNA constructs. We thank Chun Yin Lau and Fuqiang Ma in our lab for their help on bioinformatics.

The graphical abstract was created using BioRender.com. This study is supported by funds from the National Natural Science Foundation of China (Excellent Young Scientists Fund for Hong Kong and Macau, 32122002), the Research Grant Council of Hong Kong (GRF 17105523, GRF 17106322, GRF 17107021, and CRF C7026-20G), the Health Bureau of Hong Kong (HMRF 07183186 and 09201426 to C.Z.). Some strains used in this study were provided by the Caenorhabditis Genetics Center, which is funded by the NIH Office of Research Infrastructure Programs (P40 OD010440).

AUTHOR CONTRIBUTIONS

C.Z. and C.W. conceived the study and wrote the manuscript. C.W. and M.Y. carried out most of the experiments. D.L. made some constructs and performed the RNA-seq analysis. C.Z. secured funding and supervised the project. All of the authors read and approved the manuscript.

DECLARATION OF INTERESTS

The authors declare no competing interests.

Received: July 31, 2023
Revised: January 14, 2024
Accepted: February 8, 2024
Published: February 26, 2024

REFERENCES

1. Singh, A., Dawson, T.M., and Kulkarni, S. (2021). Neurodegenerative disorders and gut-brain interactions. J. Clin. Invest. *131*, e143775. https://doi.org/10.1172/JCI143775.
2. Scheperjans, F., Aho, V., Pereira, P.A.B., Koskinen, K., Paulin, L., Pekkonen, E., Haapaniemi, E., Kaakkola, S., Eerola-Rautio, J., Pohja, M., et al. (2015). Gut microbiota are related to Parkinson's disease and clinical phenotype. Mov. Disord. *30*, 350–358. https://doi.org/10.1002/mds.26069.
3. Poewe, W., Seppi, K., Tanner, C.M., Halliday, G.M., Brundin, P., Volkmann, J., Schrag, A.E., and Lang, A.E. (2017). Parkinson disease. Nat. Rev. Dis. Primers *3*, 17013. https://doi.org/10.1038/nrdp.2017.13.
4. Sampson, T.R., Debelius, J.W., Thron, T., Janssen, S., Shastri, G.G., Ilhan, Z.E., Challis, C., Schretter, C.E., Rocha, S., Gradinaru, V., et al. (2016). Gut Microbiota Regulate Motor Deficits and Neuroinflammation in a Model of Parkinson's Disease. Cell *167*, 1469–1480.e12. https://doi.org/10.1016/j.cell.2016.11.018.
5. Silva, Y.P., Bernardi, A., and Frozza, R.L. (2020). The Role of Short-Chain Fatty Acids From Gut Microbiota in Gut-Brain Communication. Front. Endocrinol. *11*, 25. https://doi.org/10.3389/fendo.2020.00025.
6. Unger, M.M., Spiegel, J., Dillmann, K.U., Grundmann, D., Philippeit, H., Bürmann, J., Faßbender, K., Schwiertz, A., and Schäfer, K.H. (2016). Short chain fatty acids and gut microbiota differ between patients with Parkinson's disease and age-matched controls. Parkinsonism Relat. Disord. *32*, 66–72. https://doi.org/10.1016/j.parkreldis.2016.08.019.
7. Hou, Y.F., Shan, C., Zhuang, S.Y., Zhuang, Q.Q., Ghosh, A., Zhu, K.C., Kong, X.K., Wang, S.M., Gong, Y.L., Yang, Y.Y., et al. (2021). Gut microbiota-derived propionate mediates the neuroprotective effect of osteocalcin in a mouse model of Parkinson's disease. Microbiome *9*, 34. https://doi.org/10.1186/s40168-020-00988-6.
8. Ostendorf, F., Metzdorf, J., Gold, R., Haghikia, A., and Tönges, L. (2020). Propionic Acid and Fasudil as Treatment Against Rotenone Toxicity in an In Vitro Model of Parkinson's Disease. Molecules *25*, 2502. https://doi.org/10.3390/molecules25112502.
9. Liu, J., Wang, F., Liu, S., Du, J., Hu, X., Xiong, J., Fang, R., Chen, W., and Sun, J. (2017). Sodium butyrate exerts protective effect against Parkinson's disease in mice via stimulation of glucagon like peptide-1. J. Neurol. Sci. *381*, 176–181. https://doi.org/10.1016/j.jns.2017.08.3235.

10. Qiao, C.M., Sun, M.F., Jia, X.B., Li, Y., Zhang, B.P., Zhao, L.P., Shi, Y., Zhou, Z.L., Zhu, Y.L., Cui, C., and Shen, Y.Q. (2020). Sodium Butyrate Exacerbates Parkinson's Disease by Aggravating Neuroinflammation and Colonic Inflammation in MPTP-Induced Mice Model. Neurochem. Res. *45*, 2128–2142. https://doi.org/10.1007/s11064-020-03074-3.

11. Chen, H., Meng, L., and Shen, L. (2022). Multiple roles of short-chain fatty acids in Alzheimer disease. Nutrition *93*, 111499. https://doi.org/10.1016/j.nut.2021.111499.

12. Ferrante, R.J., Kubilus, J.K., Lee, J., Ryu, H., Beesen, A., Zucker, B., Smith, K., Kowall, N.W., Ratan, R.R., Luthi-Carter, R., and Hersch, S.M. (2003). Histone deacetylase inhibition by sodium butyrate chemotherapy ameliorates the neurodegenerative phenotype in Huntington's disease mice. J. Neurosci. *23*, 9418–9427. https://doi.org/10.1523/JNEUROSCI.23-28-09418.2003.

13. Metzdorf, J., and Tönges, L. (2021). Short-chain fatty acids in the context of Parkinson's disease. Neural Regen. Res. *16*, 2015–2016. https://doi.org/10.4103/1673-5374.308089.

14. Wang, C., Lau, C.Y., Ma, F., and Zheng, C. (2021). Genome-wide screen identifies curli amyloid fibril as a bacterial component promoting host neurodegeneration. Proc. Natl. Acad. Sci. USA *118*, e2106504118. https://doi.org/10.1073/pnas.2106504118.

15. Raux, E., Lanois, A., Levillayer, F., Warren, M.J., Brody, E., Rambach, A., and Thermes, C. (1996). Salmonella typhimurium cobalamin (vitamin B12) biosynthetic genes: functional studies in S. typhimurium and Escherichia coli. J. Bacteriol. *178*, 753–767. https://doi.org/10.1128/jb.178.3.753-767.1996.

16. Giese, G.E., Walker, M.D., Ponomarova, O., Zhang, H., Li, X., Minevich, G., and Walhout, A.J. (2020). Caenorhabditis elegans methionine/S-adenosylmethionine cycle activity is sensed and adjusted by a nuclear hormone receptor. Elife *9*, e60259. https://doi.org/10.7554/eLife.60259.

17. Watson, E., Olin-Sandoval, V., Hoy, M.J., Li, C.H., Louisse, T., Yao, V., Mori, A., Holdorf, A.D., Troyanskaya, O.G., Ralser, M., and Walhout, A.J. (2016). Metabolic network rewiring of propionate flux compensates vitamin B12 deficiency in C. elegans. Elife *5*, e17670. https://doi.org/10.7554/eLife.17670.

18. Watson, E., MacNeil, L.T., Ritter, A.D., Yilmaz, L.S., Rosebrock, A.P., Caudy, A.A., and Walhout, A.J.M. (2014). Interspecies systems biology uncovers metabolites affecting C. elegans gene expression and life history traits. Cell *156*, 759–770. https://doi.org/10.1016/j.cell.2014.01.047.

19. McCalley, S., Pirman, D., Clasquin, M., Johnson, K., Jin, S., and Vockley, J. (2019). Metabolic analysis reveals evidence for branched chain amino acid catabolism crosstalk and the potential for improved treatment of organic acidurias. Mol. Genet. Metab. *128*, 57–61. https://doi.org/10.1016/j.ymgme.2019.05.008.

20. Yao, V., Kaletsky, R., Keyes, W., Mor, D.E., Wong, A.K., Sohrabi, S., Murphy, C.T., and Troyanskaya, O.G. (2018). An integrative tissue-network approach to identify and test human disease genes. Nat. Biotechnol. *36*, 1091–1099. https://doi.org/10.1038/nbt.4246.

21. Fan, X., Zhang, L., Li, H., Chen, G., Qi, G., Ma, X., and Jin, Y. (2020). Role of homocysteine in the development and progression of Parkinson's disease. Ann. Clin. Transl. Neurol. *7*, 2332–2338. https://doi.org/10.1002/acn3.51227.

22. Na, H., Zdraljevic, S., Tanny, R.E., Walhout, A.J.M., and Andersen, E.C. (2020). Natural variation in a glucuronosyltransferase modulates propionate sensitivity in a C. elegans propionic acidemia model. PLoS Genet. *16*, e1008984. https://doi.org/10.1371/journal.pgen.1008984.

23. Catanesi, M., Brandolini, L., d'Angelo, M., Benedetti, E., Tupone, M.G., Alfonsetti, M., Cabri, E., Iaconis, D., Fratelli, M., Cimini, A., et al. (2021). L-Methionine Protects against Oxidative Stress and Mitochondrial Dysfunction in an In Vitro Model of Parkinson's Disease. Antioxidants *10*, 1467. https://doi.org/10.3390/antiox10091467.

24. Taylor, S.R., Santpere, G., Weinreb, A., Barrett, A., Reilly, M.B., Xu, C., Varol, E., Oikonomou, P., Glenwinkel, L., McWhirter, R., et al. (2021). Molecular topography of an entire nervous system. Cell *184*, 4329–4347.e23. https://doi.org/10.1016/j.cell.2021.06.023.

25. Zhang, Q., Wu, X., Chen, P., Liu, L., Xin, N., Tian, Y., and Dillin, A. (2018). The Mitochondrial Unfolded Protein Response Is Mediated Cell-Non-autonomously by Retromer-Dependent Wnt Signaling. Cell *174*, 870–883.e17. https://doi.org/10.1016/j.cell.2018.06.029.

26. Nargund, A.M., Pellegrino, M.W., Fiorese, C.J., Baker, B.M., and Haynes, C.M. (2012). Mitochondrial import efficiency of ATFS-1 regulates mitochondrial UPR activation. Science *337*, 587–590. https://doi.org/10.1126/science.1223560.

27. Martinez, B.A., Petersen, D.A., Gaeta, A.L., Stanley, S.P., Caldwell, G.A., and Caldwell, K.A. (2017). Dysregulation of the Mitochondrial Unfolded Protein Response Induces Non-Apoptotic Dopaminergic Neurodegeneration in C. elegans Models of Parkinson's Disease. J. Neurosci. *37*, 11085–11100. https://doi.org/10.1523/JNEUROSCI.1294-17.2017.

28. Andra, A., Tanigawa, S., Bito, T., Ishihara, A., Watanabe, F., and Yabuta, Y. (2021). Effects of Vitamin B12 Deficiency on Amyloid-beta Toxicity in Caenorhabditis elegans. Antioxidants *10*, 962. https://doi.org/10.3390/antiox10060962.

29. Lam, A.B., Kervin, K., and Tanis, J.E. (2021). Vitamin B12 impacts amyloid beta-induced proteotoxicity by regulating the methionine/S-adenosylmethionine cycle. Cell Rep. *36*, 109753. https://doi.org/10.1016/j.celrep.2021.109753.

30. Bulcha, J.T., Giese, G.E., Ali, M.Z., Lee, Y.U., Walker, M.D., Holdorf, A.D., Yilmaz, L.S., Brewster, R.C., and Walhout, A.J.M. (2019). A Persistence Detector for Metabolic Network Rewiring in an Animal. Cell Rep. *26*, 460–468.e4. https://doi.org/10.1016/j.celrep.2018.12.064.

31. Durieux, J., Wolff, S., and Dillin, A. (2011). The cell-non-autonomous nature of electron transport chain-mediated longevity. Cell *144*, 79–91. https://doi.org/10.1016/j.cell.2010.12.016.

32. Magistretti, P.J., and Allaman, I. (2018). Lactate in the brain: from metabolic end-product to signalling molecule. Nat. Rev. Neurosci. *19*, 235–249. https://doi.org/10.1038/nrn.2018.19.

33. Matty, M.A., Lau, H.E., Haley, J.A., Singh, A., Chakraborty, A., Kono, K., Reddy, K.C., Hansen, M., and Chalasani, S.H. (2022). Intestine-to-neuronal signaling alters risk-taking behaviors in food-deprived Caenorhabditis elegans. PLoS Genet. *18*, e1010178. https://doi.org/10.1371/journal.pgen.1010178.

34. Christine, C.W., Auinger, P., Joslin, A., Yelpaala, Y., and Green, R.; Parkinson Study Group-DATATOP Investigators (2018). Vitamin B12 and Homocysteine Levels Predict Different Outcomes in Early Parkinson's Disease. Mov. Disord. *33*, 762–770. https://doi.org/10.1002/mds.27301.

35. Dietiker, C., Kim, S., Zhang, Y., and Christine, C.W. (2019). Characterization of Vitamin B12 Supplementation and Correlation with Clinical Outcomes in a Large Longitudinal Study of Early Parkinson's Disease. J. Mov. Disord. *12*, 91–96. https://doi.org/10.14802/jmd.18049.

36. Xu, Y., Xiang, S., Ye, K., Zheng, Y., Feng, X., Zhu, X., Chen, J., and Chen, Y. (2018). Cobalamin (Vitamin B12) Induced a Shift in Microbial Composition and Metabolic Activity in an in vitro Colon Simulation. Front. Microbiol. *9*, 2780. https://doi.org/10.3389/fmicb.2018.02780.

37. Arumugam, M., Raes, J., Pelletier, E., Le Paslier, D., Yamada, T., Mende, D.R., Fernandes, G.R., Tap, J., Bruls, T., Batto, J.M., et al. (2011). Enterotypes of the human gut microbiome. Nature *473*, 174–180. https://doi.org/10.1038/nature09944.

38. Paiva, I., Pinho, R., Pavlou, M.A., Hennion, M., Wales, P., Schütz, A.L., Rajput, A., Szego, É.M., Kerimoglu, C., Gerhardt, E., et al. (2017). Sodium butyrate rescues dopaminergic cells from alpha-synuclein-induced transcriptional deregulation and DNA damage. Hum. Mol. Genet. *26*, 2231–2246. https://doi.org/10.1093/hmg/ddx114.

39. Parada Venegas, D., De la Fuente, M.K., Landskron, G., González, M.J., Quera, R., Dijkstra, G., Harmsen, H.J.M., Faber, K.N., and Hermoso, M.A. (2019). Short Chain Fatty Acids (SCFAs)-Mediated Gut Epithelial and Immune Regulation and Its Relevance for Inflammatory Bowel

Diseases. Front. Immunol. *10*, 277. https://doi.org/10.3389/fimmu.2019.00277.

40. Forsyth, C.B., Shannon, K.M., Kordower, J.H., Voigt, R.M., Shaikh, M., Jaglin, J.A., Estes, J.D., Dodiya, H.B., and Keshavarzian, A. (2011). Increased intestinal permeability correlates with sigmoid mucosa alpha-synuclein staining and endotoxin exposure markers in early Parkinson's disease. PLoS One *6*, e28032. https://doi.org/10.1371/journal.pone.0028032.
41. Haghikia, A., Jörg, S., Duscha, A., Berg, J., Manzel, A., Waschbisch, A., Hammer, A., Lee, D.H., May, C., Wilck, N., et al. (2015). Dietary Fatty Acids Directly Impact Central Nervous System Autoimmunity via the Small Intestine. Immunity *43*, 817–829. https://doi.org/10.1016/j.immuni.2015.09.007.
42. Brown, A.J., Goldsworthy, S.M., Barnes, A.A., Eilert, M.M., Tcheang, L., Daniels, D., Muir, A.I., Wigglesworth, M.J., Kinghorn, I., Fraser, N.J., et al. (2003). The Orphan G protein-coupled receptors GPR41 and GPR43 are activated by propionate and other short chain carboxylic acids. J. Biol. Chem. *278*, 11312–11319. https://doi.org/10.1074/jbc.M211609200.
43. Bargmann, C.I. (1998). Neurobiology of the Caenorhabditis elegans genome. Science *282*, 2028–2033. https://doi.org/10.1126/science.282.5396.2028.
44. Candido, E.P., Reeves, R., and Davie, J.R. (1978). Sodium butyrate inhibits histone deacetylation in cultured cells. Cell *14*, 105–113. https://doi.org/10.1016/0092-8674(78)90305-7.
45. Sealy, L., and Chalkley, R. (1978). The effect of sodium butyrate on histone modification. Cell *14*, 115–121. https://doi.org/10.1016/0092-8674(78)90306-9.
46. Duscha, A., Gisevius, B., Hirschberg, S., Yissachar, N., Stangl, G.I., Dawin, E., Bader, V., Haase, S., Kaisler, J., David, C., et al. (2020). Propionic Acid Shapes the Multiple Sclerosis Disease Course by an Immunomodulatory Mechanism. Cell *180*, 1067–1080.e16. https://doi.org/10.1016/j.cell.2020.02.035.
47. Lakso, M., Vartiainen, S., Moilanen, A.M., Sirviö, J., Thomas, J.H., Nass, R., Blakely, R.D., and Wong, G. (2003). Dopaminergic neuronal loss and motor deficits in Caenorhabditis elegans overexpressing human alpha-synuclein. J. Neurochem. *86*, 165–172. https://doi.org/10.1046/j.1471-4159.2003.01809.x.
48. Brenner, S. (1974). The genetics of Caenorhabditis elegans. Genetics *77*, 71–94. https://doi.org/10.1093/genetics/77.1.71.
49. Adams, F.S., La Rosa, F.G., Kumar, S., Edwards-Prasad, J., Kentroti, S., Vernadakis, A., Freed, C.R., and Prasad, K.N. (1996). Characterization and transplantation of two neuronal cell lines with dopaminergic properties. Neurochem. Res. *21*, 619–627. https://doi.org/10.1007/BF02527762.
50. Kamath, R.S., Fraser, A.G., Dong, Y., Poulin, G., Durbin, R., Gotta, M., Kanapin, A., Le Bot, N., Moreno, S., Sohrmann, M., et al. (2003). Systematic functional analysis of the Caenorhabditis elegans genome using RNAi. Nature *421*, 231–237. https://doi.org/10.1038/nature01278.
51. Winston, W.M., Molodowitch, C., and Hunter, C.P. (2002). Systemic RNAi in C. elegans requires the putative transmembrane protein SID-1. Science *295*, 2456–2459. https://doi.org/10.1126/science.1068836.
52. Datsenko, K.A., and Wanner, B.L. (2000). One-step inactivation of chromosomal genes in Escherichia coli K-12 using PCR products. Proc. Natl. Acad. Sci. USA *97*, 6640–6645. https://doi.org/10.1073/pnas.120163297.
53. Finney, M., and Ruvkun, G. (1990). The unc-86 gene product couples cell lineage and cell identity in C. elegans. Cell *63*, 895–905. https://doi.org/10.1016/0092-8674(90)90493-x.
54. Fatouros, C., Pir, G.J., Biernat, J., Koushika, S.P., Mandelkow, E., Mandelkow, E.M., Schmidt, E., and Baumeister, R. (2012). Inhibition of tau aggregation in a novel Caenorhabditis elegans model of tauopathy mitigates proteotoxicity. Hum. Mol. Genet. *21*, 3587–3603. https://doi.org/10.1093/hmg/dds190.
55. Luz, A.L., Rooney, J.P., Kubik, L.L., Gonzalez, C.P., Song, D.H., and Meyer, J.N. (2015). Mitochondrial Morphology and Fundamental Parameters of the Mitochondrial Respiratory Chain Are Altered in Caenorhabditis elegans Strains Deficient in Mitochondrial Dynamics and Homeostasis Processes. PLoS One *10*, e0130940. https://doi.org/10.1371/journal.pone.0130940.

STAR★METHODS

KEY RESOURCES TABLE

REAGENT or RESOURCE	SOURCE	IDENTIFIER
Antibodies		
Mouse monoclonal anti-α-syn antibody	abcam	Cat# ab27766; RRID:AB_727020
Rhodamine-conjugated goat anti-mouse IgG antibody	Jackson Lab	Cat# 115-025-164; RRID: AB_2338489
Mouse monoclonal anti-α-Tubulin Antibody	abcam	Cat# ab7291; RRID: AB_2241126
Rabbit anti-Tyrosine Hydroxylase Antibody	Merck	Cat# AB152; RRID: AB_390204
Goat anti-Rabbit IgG (H + L) Highly Cross-Adsorbed Secondary Antibody, Alexa Fluor™ Plus 488	Thermo Fisher	Cat# A32731; RRID: AB_2633280
Bacterial and virus strains		
Escherichia coli OP50	Caenorhabditis Genetics Center (CGC)	OP50
Escherichia coli K12 Keio Knockout Collection	Dharmacon	OEC4988
Comamonas aquatic DA1877	CGC	DA1877
Escherichia coli K12 wild type (Keio library Parental Strain)	Dharmacon	BW25113
Escherichia coli K12 *ΔcobS:Kana; ΔcobA:Cm*	This study	*cobA(−) cobS(−)*
Chemicals, peptides, and recombinant proteins		
Sodium propionate	Merck	P1880
Propionic acid	Merck	P1386
Coenzyme B12	Merck	C0884
Ammonium formate	Honeywell	#55674
Fetal Bovine Serum, qualified, heat inactivated, Brazil	Thermo Fisher	10500064
DMEM/F-12, HEPES, powder, 1L	Thermo Fisher	42400010
RPMI 1640 Medium (1X), liquid, With 25mM HEPES & L-Glutamine	Merck	SLM-140-B
Fetal Bovine Serum, US Origin, EmbryoMax® ES Cell Qualified FBS	Merck	ES-009-B
Dibutyryl-cAMP	Sigma Aldrich	28745-25mg
Dehydroepiandrosterone solution	Shanghai Aladdin	D121747-1mg
EmbryoMax® L-Glutamine Solution (100X), 200mM	Merck	TMS-002-C
Lipofectamine™ Transfection Reagent	Thermo Fisher	18324012
2 × Phanta Max Master Mix	Vazyme	P515-03
ClonExpress Ultra One Step Cloning Kit	Vazyme	C115-02
SuperScript II Reverse Transcriptase	Thermo Fisher	18064071
SYBR® Premix Ex Taq™ (Tli RNaseH Plus)	Takara	RR420A
Critical commercial assays		
Seahorse XFe24 FluxPak mini	Agilent	102342–100
Cell Counting Kit 8 (WST-8/CCK8)	abcam	ab228554
Deposited data		
RNA-seq raw data	This study	GEO: GSE230786
Experimental models: Cell lines		
Human neuroblastoma cell line SH-SY5Y	ATCC	Cat# CRL-2266; RRID: CVCL_0019
N27 Rat Dopaminergic Neural Cell Line	Sigma-Aldrich	Cat# SCC048; RRID: CVCL_D584
Experimental models: Organisms/strains		
Caenorhabditis elegans: N2 (wild type)	CGC	N2
C. elegans: VL749 *wwIs24[acdh-1p::GFP + unc-119(+)]*	CGC	VL749

(*Continued on next page*)

Continued

REAGENT or RESOURCE	SOURCE	IDENTIFIER
C. elegans: SJ4100 *zcIs13[hsp-6p::GFP + lin-15(+)] V.*	CGC	SJ4100
C. elegans: CLP215 *twnEx8[mec-7p::tomm-20::mCherry + myo-2p::GFP]*	CGC	CLP215
C. elegans: AM101 *rmIs110[F25B3.3p::Q40::YFP]*	CGC	AM101
C. elegans: UM10 *unkIs7[aex-3p::α-syn(A53T), dat-1p::gfp]*	Gift from Prof. Garry Wong[47]	UM10
C. elegans: UM6 *unkIs9[dat-1p::α-syn(A53T), dat-1p::gfp]*	Gift from Prof. Garry Wong[47]	UM6
C. elegans: CGZ621 *unkIs11[dat-1p::GFP]*	Gift from Prof. Garry Wong[47]	P_{dat-1}*::GFP*
C. elegans: CGZ1578 *wwIs24 [acdh-1p::GFP + unc-119(+)]; unkEx285[rab-3p::Abeta1-42; myo-2p::mCherry]*	This study	CGZ1578
C. elegans: CGZ1579 *wwIs24 [acdh-1p::GFP + unc-119(+)]; unkEx440[myo-3p::Abeta1-42; myo-2p::mCherry]*	This study	CGZ1579
C. elegans: CGZ1087 *wwIs24 [acdh-1p::GFP + unc-119(+)]; unkEx251[myo-3p::asyn A53T;myo-2p::mCherry]*	This study	CGZ1087
C. elegans: CGZ1048 *wwIs24[acdh-1p::GFP]; unkEx237[rab-3p::nhr-68; rab-3p::nhr-114; myo-2p::mCherry]*	This study	CGZ1048
C. elegans: CGZ1047 *wwIs24[acdh-1p::GFP]; unkEx239[dat-1p::nhr-68; dat-1p::nhr-114; myo-2p::mCherry]*	This study	CGZ1047
C. elegans: CGZ1046 *wwIs24[acdh-1p::GFP]; unkEx236[ges-1p::nhr-68; ges-1p::nhr-114; myo-2p::mCherry]*	This study	CGZ1046
C. elegans: CGZ1044 *unkIs7[aex-3p::alpha-synuclein A53T; dat-1p::gfp] IV; unkEx236[ges-1p::nhr-68; ges-1p::nhr-114; myo-2p::mCherry]*	This study	CGZ1044
C. elegans: CGZ1065 *unkIs7; wwIs24[acdh-1p::GFP]; unkEx237[rab-3p::nhr-68; rab-3p::nhr-114; myo-2p::mCherry]*	This study	CGZ1065
C. elegans: CGZ1063 *unkIs7; wwIs24[acdh-1p::GFP]; unkEx238[ges-1p::nhr-68; ges-1p::nhr-114; myo-2p::mCherry]*	This study	CGZ1063
C. elegans: CGZ1075 *unkIs7; unkEx237[rab-3p::nhr-68; rab-3p::nhr-114; myo-2p::mCherry]*	This study	CGZ1075
C. elegans: CGZ1074 *unkIs7; unkEx236[dat-1p::nhr-68; dat-1p::nhr-114; myo-2p::mCherry]*	This study	CGZ1074
C. elegans: CGZ1461 *unkIs7; unkEx385[ges-1p::bcat-1; ges-1p::cth-1; ges-1p::cth-2; myo-2p::mCherry]*	This study	CGZ1461
C. elegans: CGZ1462 *unkIs7; unkEx386[ges-1p::bcat-1; myo-2p::mCherry]*	This study	CGZ1462
C. elegans: CGZ1464 *unkIs7; unkEx388[rab-3p::bcat-1; myo-2p::mCherry]*	This study	CGZ1464
C. elegans: CGZ1086 *unkIs7; nhr-68(gk708)*	This study	CGZ1086
C. elegans: CGZ1608 *unkIs7; atfs-1(gk3094)*	This study	CGZ1608
C. elegans: CGZ1793 *unkIs7; wwIs24[acdh-1p::GFP + unc-119(+)]; unkEx557[ges-1p::atfs-1 RNAi; myo-2p::mCherry]*	This study	CGZ1793
C. elegans: CGZ1794 *unkIs7; atfs-1(gk3094); wwIs24[acdh-1p::GFP]; unkEx558[ges-1p::atfs-1; myo-2p::mCherry]*	This study	CGZ1794
C. elegans: CGZ1617 *unkIs7; daf-2(e1370)*	This study	CGZ1617
C. elegans: CGZ1778 *unkIs7; daf-2(e1370); unkEx543[rab-3p::daf-2; myo-2p::mCherry]*	This study	CGZ1778
C. elegans: CGZ1779 *unkIs7; daf-2(e1370); unkEx544[ges-1p::daf-2; myo-2p::mCherry]*	This study	CGZ1779
C. elegans: CGZ1825 *unkIs7; tph-1(mg280) II; wwIs24[acdh-1p::GFP]*	This study	CGZ1825
C. elegans: CGZ1861 *wwIs24 [acdh-1p::GFP + unc-119(+)]; egl-20(n585); unkEx582[rab-3p::a-syn(A53T); myo-2p::mCherry]*	This study	CGZ1861

(*Continued on next page*)

Continued

REAGENT or RESOURCE	SOURCE	IDENTIFIER
C. elegans: CGZ1796 *unkIs7; unkEx559[rab-3p::ldh-1; myo-2p::mCherry]*	This study	CGZ1796
C. elegans: CGZ1797 *unkIs7; unkEx560[ges-1p::ldh-1; myo-2p::mCherry]*	This study	CGZ1797
C. elegans: CGZ833 *unkIs7; twnEx8[mec-7p::tomm-20::mCherry; myo-2p::GFP]*	This study	CGZ833
C. elegans: CGZ1795 *unkIs7; twnEx8; unkEx385[ges-1p::bcat-1; ges-1p::cth-1; ges-1p:: cth-2;myo-2p::mCherry]*	This study	CGZ1795
Oligonucleotides		
List of Oligonucleotides used	This study	Table S8
Recombinant DNA		
pHM6-α-syn(A53T)	Addgene	#40825
Pmax-GFP	Addgene	#71886
pKD46	Gift from Dr. Aixin Yan	pKD46
pBSK-lcml-3FLAG	Gift from Dr. Aixin Yan	N/A
rab-3p::Abeta::unc-54 3′UTR	This study	CGZ#438
myo-3p::Abeta::unc-54 3′UTR	This study	CGZ#508
ges-1p::bcat-1::unc-54_3′UTR	This study	CGZ#599
ges-1p::cth-1::unc-54 3′UTR	This study	CGZ#600
ges-1p::cth-2::unc-54 3′UTR	This study	CGZ#601
rab-3p::bcat-1::unc-54 3′UTR	This study	CGZ#609
dat-1p::nhr-68::unc-54 3′UTR	This study	CGZ#368
ges-1p::nhr-68::unc-54 3′UTR	This study	CGZ#376
rab-3p::nhr-68::unc-54 3′UTR	This study	CGZ#381
acdh-1p::gfp::H2B::unc-54 3′UTR	This study	CGZ#348
rab-3p::ldh-1::unc-54 3′UTR	This study	CGZ#771
ges-1p::ldh-1::unc-54 3′UTR	This study	CGZ#773
ges-1p::atfs-1_sense(noATG)::unc-54 3′UTR	This study	CGZ#772
ges-1p::atfs-1_antisense::unc-54 3′UTR	This study	CGZ#783
ges-1p::atfs-1(+)::unc-54 3′UTR	This study	CGZ#785
Software and algorithms		
ImageJ	NIH	https://imagej.nih.gov/ij/
GraphPad Prism 8.0	GraphPad Software, Inc.	https://www.graphpad.com/scientific-software/prism/
STAR 2.7.10a	Github	https://github.com/alexdobin/STAR
R (V4.3)	R-project	https://www.r-project.org
DESeq2 (1.38.1)	Bioconductor	https://bioconductor.org/packages/release/bioc/html/DESeq2.html
dplyr (1.0.10)	R package	https://dplyr.tidyverse.org
Leica Application Suite X (3.7.6.25997)	Leica Microsystems	https://www.leica-microsystems.com/products/microscope-software/p/leica-las-x-ls/downloads/

RESOURCE AVAILABILITY

Lead contact

Further information and requests for resources and reagents should be directed to and will be fulfilled by the lead contact, Chaogu Zheng (cgzheng@hku.hk).

Materials availability

Strains and plasmids generated in this study will be shared by the lead contact upon request.

Data and code availability

- RNA-seq data have been deposited to GEO and are publicly available. Accession numbers are listed in the key resources table. Our analysis of the differentially expressed genes between various conditions are reported in the supplemental tables.
- This paper does not report original code.
- Any additional information required to reanalyze the data reported in this paper is available from the lead contact upon request.

EXPERIMENTAL MODEL AND STUDY PARTICIPANT DETAILS

C. elegans strains

C. elegans wild-type (N2) and mutant strains were maintained at 20°C using the standard culturing protocol.[48] PD strains UM10 *unkIs7[aex-3p::α-syn(A53T), dat-1p::gfp]* and UM6 *unkIs9 [dat-1p::α-syn(A53T), dat-1p::gfp]* and the wild-type control strain carrying *unkIs11[dat-1p::gfp]* were generous gifts from Garry Wong, Faculty of Health Sciences, University of Macau, Macau, China. The polyQ strain AM101 *rmIs110[F25B3.3p::Q40::YFP]*, *acdh-1* reporter VL749 *wwIs24 [acdh-1p::GFP + unc-119(+)]*, mitoUPR reporter SJ4100 *zcIs13[hsp-6::GFP + lin-15(+)] V*, mitochondrial morphological marker CLP215 *twnEx8[mec-7p::tomm-20::mCherry + myo-2p::GFP]*, VC3201 *atfs-1(gk3094) V*, CB1370 *daf-2(e1370) III*, MT15434 *tph-1(mg280) II*, and MT1215 *egl-20(n585) IV* were obtained from the Caenorhabditis Genetics Center.

Cell lines and culture conditions

The human neuroblastoma SH-SY5Y cells were maintained in DMEM/F12 (1:1; Thermo Fisher) supplemented with Fetal Bovine Serum (10% v/v). The N27 rat dopaminergic neural cells[49] were maintained in RPMI1640 (containing HEPES and L-glutamine) supplemented with 10% ES cell qualified FBS (Merck) and 1% L-Glutamine (Merck). To differentiate N27 cells into dopaminergic neurons, cells were seeded into 96-well plates precoated with 0.01% poly-*d*-lysine at a density of 1×10^4 cells/well in the culture medium. 24 h later, the medium was changed to a culture medium containing 30 μg/mL dehydroepiandrosterone (Aladdin) and 1 mg/mL dibutyryl-cAMP (Sigma), and cells were allowed to differentiate for 3 days. Immunofluorescence using anti-tyrosine hydroxylase (TH) antibody (Merck) was performed to confirm the successful differentiation.

METHOD DETAILS

Constructs, transgenes, and RNAi

A 2 kb *ges-1* promoter (cloned from N2 genomic DNA) was used to drive intestine-specific expression, and a 1.2 kb *rab-3* promoter (subcloned from pGH8 *rab-3p::mCherry* obtained from Addgene) was used to drive pan-neuronal expression, and a 0.7 kb *dat-1* promoter (subcloned from a *dat-1p::α-syn* construct provided by Garry Wong) was used to drive DA-specific expression. The genomic coding regions of *bcat-1, cth-1, cth-2, nhr-68*, *nhr-114*, *atfs-1*, and *ldh-1* were cloned from N2 genomic DNA and ligated to the downstream of desired promoters using Gibson Assembly method with the ClonExpress kit from Vazyme Biotech (Nanjing, China). The *myo-3p::α-syn(A53T)* construct was created by swapping the *dat-1* promoter in the *dat-1p::α-syn(A53T)* construct with a 2.5 kb *myo-3* promoter. The *rab-3::Aβ* construct was generated by replacing the mCherry with a synthesized Aβ1-42 coding sequence into pGH8 via site-directed mutagenesis; the *rab-3* promoter is then replaced by a *myo-3* promoter to make the *myo-3p::Aβ* construct. A 2.9 kb *acdh-1* promoter was used to drive the expression of *gfp::his-58* to make *acdh-1p::GFP::H2B*.

To generate transgenic animals, we injected DNA constructs (15–20 ng/μL) with a co-injection marker *myo-2p::mCherry* into the PD animals. The resulted stable lines were scored for Unc phenotype and ADE loss. Intestine-specific *atfs-1* RNAi was done by cloning the sense and antisense sequence of *atfs-1* (without the start codon), placing them downstream of the *ges-1* promoter, and then injecting the two constructs together into worms to create a transgene that expressed dsRNA against *atfs-1* only in the intestine. RNAi against *cco-1* was delivered through bacterial feeding.[50] HT115 bacteria expressing dsRNA against *cco-1* was obtained from the Ahringer library[50] and were grown overnight on NGM plates containing 5 mM IPTG with or without 10 mM propionic acid. Eggs of SJ4100 animals were then seeded onto these RNAi plates to test the effects on *hsp-6p::GFP* expression. Since dsRNA is transported into *C. elegans* cells through the transmembrane protein SID-1 and neurons do not express *sid-1*,[51] feeding RNAi against *cco-1* does not affect neurons and causes intestinal mitoUPR cell-autonomously. Primers used for cloning can be found in Table S8.

Construction of double knockout K12 *E. coli* bacteria

We used an established λ red recombineering protocol[52] to generate *cobA(−); cobS(−)* double knockout mutants in *E.coli* K12. We first used primers carrying ~50 bp of *cobA*-flanking sequences (Table S8) to amplify a chloramphenicol (Cm) resistance gene to generate the repair template. We transformed the *cobS(−)* single knockout bacteria from the Keio collection with λ red expression plasmid pKD46 and then grow the bacteria until OD600 reaches 0.4–0.6 in the presence of L-Arabinose at 30°C. We then washed the cells with ice-cold 10% glycerol to make electrocompetent cells, which were mixed with the purified PCR products and

electroporated at 2.0 kV. Cells were then plated on LB agar plates containing Cm. Colonies were verified by colony PCR and Sanger sequencing.

Immunofluorescence and fluorescent imaging

Antibody staining was performed using the Ruvkun protocol.[53] Briefly, PD animals fed with different bacteria were fixed in fixation buffer with 2% formaldehyde in liquid nitrogen, subjected to several freeze-thaw cycles, and then treated with reducing and oxidizing agents to break the cuticle. To detect α-syn, the mouse monoclonal anti-α-syn antibody (ab27766, Abcam; 1:500 dilution) was incubated with the PD animals at 4°C overnight with rotation. Rhodamine-conjugated goat anti-mouse IgG antibody (115-025-164, Jackson Lab; 1:1000) was used as secondary antibody. After washing, the animals were mounted on agarose pads for visualization.

For the ADE degeneration assays, about 30 L1 animals of the PD strains were placed on NGM plates with bacteria and chemicals of interest. Animals were scored as day-2 adults for the percentage of animals showing two ADE neurons that were clearly labeled by GFP and had normal cell morphology. Fluorescent imaging was performed on a Leica DMi8 inverted microscope equipped with a Leica K5 monochrome camera. The Leica THUNDER deconvolution system was used to process some images to increase the clarity of the pictures and remove out-of-focus light. Measurements were made using the Leica Application Suite X (3.7.6.25997) software.

Sequential fractionation and western blot

To measure the level of α-syn in high-salt soluble, detergent soluble and insoluble fractions of worm lysate, sequential fractionation was performed according to published methods.[54] Briefly, synchronized worms were pelleted and resuspended in high-salt RAB buffer [100 mM 2-(N-morpholino) ethanesulfonic acid (MES), 1 mM EGTA, 0.5 mM $MgSO_4$, 20 mM NaF] and then lysed by sonication (6 × 10 s, 10 s break). The lysate was then centrifuged at 40,000×g for 40 min at 4°C; the supernatant constituted the RAB fraction. The pellet was re-extracted with 1 M sucrose in RAB buffer and the supernatant was discarded. The pellet was then extracted with RIPA buffer (150 mM NaCl, 1% Nonidet P-40, 0.5% deoxycholate, 0.1% SDS, 50 mM Tris, pH 8.0) and centrifuged at 40,000×g for 20 min at 4°C to produce the supernatant as the RIPA fraction. The pellet, after a brief washing with RIPA buffer, was extracted with 30% formic acid (FA) and centrifuged at 13,000×g for 15 min at room temperature; the supernatant became the FA fraction. All buffers contained the Roche cOmplete Protease Inhibitor cocktail and 0.5 mM PMSF. The pH of FA fraction was adjusted by 5M NaOH. All fractions were subjected to western blot analysis using anti-α-syn (ab27766, Abcam; 1:1000 dilution) and anti-tubulin (ab7291, Abcam; 1:2000 dilution) antibodies. The intensity of the bands was measured by ImageJ software.

Behavioral assays

For locomotion assessment, about 30 synchronized L1 animals of the UM10 strain with pan-neuronal expression of α-syn A53T were placed on NGM plates with bacteria and chemicals of interest and grown for 48 h at 20°C. The penetrance of non-Unc phenotype was then scored at L4 stage. The animals that traced smooth, sinuous waves were considered non-Unc, and the animals that made irregular bends or kinks along their bodies were considered Unc. For the basal slowing response assays, young adults grown under desired conditions were transferred to unseeded NGM plate or plates with *E. coli* OP50. Worms were allowed to acclimate to the assay plates for 5 min, and then the number of body bends per 20 s was counted for each animal.

Mass spectrometry

The quantification of VB12 in bacterial lysate and *C. elegans* lysate was performed using LC-MS/MS system consisting of an ultra-high pressure LC system (Agilent 1290) equipped with AB SCIEX 3200 QTRAP according to a published study.[18] Briefly, bacteria or worm cultures were harvested, washed twice with 50 mM sodium citrate buffer (pH = 7.2), and treated with 3 mL of 100 mM sodium acetate buffer (pH = 4.0) containing 2 mg porcine pepsin for 3 h at 37°C with agitation. The extract was clarified by centrifugation and purified using a gravity drip C18 100 mg column (8B-S001-EBJ, Phenomenex, Inc). The column was preconditioned with 3 mL methanol, followed by 3 mL water. The samples were then applied onto the columns, which was subsequently washed with 3 mL water and eluted with 1.5 mL methanol. The samples were dried under vacuum and resuspended in water corresponding to 0.5 OD600 unit of cells per mL of solution. We used an Agilent UHPLC system, HTS PAL autosampler, and an Agilent 6490 QQQ using phenyl-hexyl UHPLC column 2.1 × 100 mm, 1.7 μm particle size (00D-4500-AN, Phenomenex) to perform LC-MS analysis. Mobile phase A was 20 mM ammonium formate with 0.1% formic acid in water. Mobile phase B was 20 mM ammonium formate and 0.1% formic acid in methanol. The gradient was 0 min, 10% B, 0.5 min 33% B, 3 min 50% B, 3.1 min 90% B, 3.5 min 90% B, 4 min 10% A, supplied throughout at 0.5 mL/min. The column temperature was maintained at 35°C and the autosampler at 4°C. The injection loop volume was 2 mL. The QQQ was run in positive ionization mode. Instrument run parameters were set as the following: nebulizer pressure 20 psi, source gas temp 290°C, source gas flow 13 LPM, sheath gas temp 400°C, sheath gas flow 12 LPM, capillary voltage 3000 V, nozzle voltage 1000V, high pressure funnel RF 190V, low pressure funnel RF 100V. Monitored parent/product ions (collision energy) was 790.6/147.2 (50). Adenosylcobalamin was separated with a retention time of 2.3 min. Standards were purchased from Sigma-Aldrich and prepared freshly in water for analysis.

Homocysteine was also detected by LC-MS/MS after being selectively derivatized by 50 mM N-ethylmaleimide (NEM) in water. Samples were then dried under speed vac and reconstituted in 80% methanol/water (v/v). The LC-MS/MS was carried out on an Acquity I-Class ultra-high-performance LC system by Waters (Milford, MA, USA). Mobile phases used were 0.1% formic acid (A) and acetonitrile (B). The column was a Phenomenex Synergi 4 μm Fusion-RP 80 Å (2 mm × 50 mm). The injection volume was

5 μL and flow rate 0.5 mL/min. The column temperature was set at 40°C. The gradient condition started at 0% phase B (hold time 0.1 min) and was increased to 10% B at 1 min, then to 50% B at 6.5 min, and finally to 100% B at 7 min (hold time 1 min). The gradient was re-equilibrated to 0% phase B for 2 min. The mass spectrometry analysis was processed using a QTRAP6500+ from AB Sciex (Framingham, MA, USA). Electrospray ionization parameters were as follows: electrospray voltage of +4500V, temperature of 550°C, curtain gas of 25, CAD gas medium, and gas 1 and 2 of 45 and 50 psi, respectively.

Other metabolites were quantified through metabolomic studies conducted by BGI (Shenzhen, China). 10 mg of synchronized animals fed with K12 WT or *cobA(−); cobS(−)* bacteria were ground, and 20 μL of the lysate was mixed with 20 μL of the standard and 120 μL of sample releasing agent. The mixture was then incubated for 30 min with shaking and centrifuged at 18,000 g at 4°C for 30 min; 30 μL of the supernatant was then transferred to a 96-well plate, in which 20 μL of derivatization reagent and 20 μL of EDC working solution were added. The plate was allowed to react at 40°C with shaking (1,200 rpm) for 60 min and then centrifuged at 4,000 g at 4°C for 5 min. 30 μL of the reaction was transferred to a new 96-well plate, and 90 μL sample diluent was added to each well. The plate was incubated for 10 min with shaking (600 rpm), centrifuged at 4,000 g at 4°C for 30 min, sealed with film, and ready for LC-MS/MS. The sample extracts were analyzed using Waters UPLC I-Class Plus (Waters, USA) equipped with QTRAP 6500 Plus (SCIEX, USA). For chromatography, the column used is BEH C18 (2.1 mm × 10 cm, 1.7 μm, waters). The Mobile phase A is water containing 0.1% formic acid. The Mobile phase B is acetonitrile containing 30% isopropanol. Elution was performed using the following gradient: 0 min, 5% B; 1 min, 5% B; 5 min, 70% B; 9 min, 50% B; 11 min, 22% B; 13.5 min, 95% B (the flow speed from 0 to 14 min is 0.4 mL/min); 14 min, 100% B (0.6 mL/min); 16 min, 5% B (0.4 mL/min). The column temperature is 40°C. For Mass Spectrometry, a QTRAP 6500 Plus with ESI Turbo ion spray interface was used with the following parameters. Ion source temperature: 400°C; ion spray voltage: 4500V and −4500V; ion source gas 1, ion source gas 2, and curtain gas were set to 60, 60, and 35 psi, respectively. The MRM mode was set to include the parent-daughter transition information of target metabolites, collision energy, declustering potential, and retention time.

RNA-seq and RT-qPCR

Total RNA from *C. elegans* was extracted using TRIzol reagent (Thermo Fisher). Samples were sent to BGI (Beijing Genome Institutes, Shenzhen, China) for standard library construction and pair-end sequencing. Around 20 million reads were obtained for each sample, and the reads were aligned to the *C. elegans* genome (WS235) using STAR 2.7. To identify genes differentially expressed, the transcript counts were analyzed using DESeq2, and genes with false discovery rate–corrected p values below 0.05 and fold change above 2 or below 0.5 were identified. Gene enrichment analysis was then performed on the genes showing significant changes in expression levels using the DAVID functional annotation tool (2021 version). CGZ621 *unkIs11[dat-1p::gfp]* animals were used as the wild-type control for comparison with the UM10 and UM6 PD animals, which also carry a *dat-1p::gfp* transgene.

For transcriptional analysis, cDNA was reversed transcribed from total RNA using SuperScript II Reverse Transcriptase (Thermo Fisher) from synchronized L4 animals. Quantitative real-time PCR was performed using a TB Green Premix Ex Taq kit (Takara) in a CFX96 real-time PCR machine (BioRad). Values were first normalized to the internal control *ama-1*, and the fold change was then calculated by comparing the normalized data of various treatment with the wild-type control. All data shown represent the average of three biologically independent replicates. The qPCR primers are listed in Table S8.

Mitochondrial respiration assay

For mitochondrial cellular respiration assay, oxygen consumption rate (OCR) was measured using the Agilent Seahorse XFe24 technology.[55] Briefly, the sensor cartridges were hydrated in Seahorse calibration buffer at 25°C overnight before the experiment. Day-one adults were washed with complete K-medium and suspended in 525 μL of unbuffered EPA water. About 50–100 animals were added into each well of the Agilent Seahorse microplate. To achieve equivalent volume after compound injection, we loaded 75 μL of 160 μM DCCD (8×), 225 μM FCCP (9×) and 100 mM sodium azide (10×) in Port A, B, and C, respectively. The basal respiration was first measured in every well, followed by the injection of FCCP in half of the wells and DCCD in the other half. Sodium azide was injected at the end of the assay in every well to completely block mitochondrial respiration. The number of measurements for basal respiration, DCCD, FCCP, and sodium azide responses were set to 8, 14, 8 and 4, respectively. ATP-linked respiration is calculated by subtracting DCCD response from the basal OCR. FCCP response reflects the maximal respiratory capacity, while non-mitochondrial respiration is defined as the OCR after adding the azide. All data were normalized by the number of animals.

Mammalian cell culture and cell viability assay

The human neuroblastoma SH-SY5Y cells were first transfected with pHM6-α-syn (A53T) or the control plasmid (Pmax-GFP) for 24 h and then cultured with or without sodium propionate and VB12 in 96-well plates at a density of 1×10^4 cells/well and grown for 24 h. Cell viability was then determined using the cell counting kit 8 (CCK-8, Abcam); 10 μL of CCK-8 solution was added to each well, and the absorbance was measured at 460 nm on a SpectraMax iD3 multi-mode microplate reader (Molecular Devices) 1 h later. Cell viability was calculated using the following formula:

$$\text{Viability } \% = \frac{Absorbance_{exp.} - Mean\left(Absorbance_{neg.ctlr}\right)}{Mean\left(Absorbance_{pos.ctrl}\right)} * 100$$

At least five replicates were performed for each condition, and the mean ± SD were plotted.

Similarly, N27 cells were differentiated for three days and then transfected with pHM6-α-syn (A53T); sodium propionate and VB12 were added at 12 h after the transfection. 48 h later, cell viability was measured using the CCK-8 kit.

QUANTIFICATION AND STATISTICAL ANALYSIS

All quantitative data were shown as mean ± SD of at least three biological replicates. For statistical analysis, we used a one-way ANOVA followed by a Dunnett's multiple comparisons test of different treatments with a single control group or a Tukey's honestly significant difference (HSD) test for all pairs of conditions. A two-tailed Student's *t* test was used to compare only two groups, and the p values obtained were then corrected by a Bonferroni correction. Single asterisks indicate statistical significance at $p < 0.05$, and double asterisk for $p < 0.01$. All statistical analyses were carried out using GraphPad Prism 8.0 software. Statistical details of experiments and sample sizes can be found in the figure legends.